

RESEARCH ARTICLE

Depletion of *M. tuberculosis* GlmU from Infected Murine Lungs Effects the Clearance of the Pathogen

Vijay Soni^{1,2}, Sandeep Upadhayay¹, Priyanka Suryadevara², Ganesh Samla², Archana Singh³, Perumal Yogeewari², Dharmarajan Sriram², Vinay Kumar Nandicoori^{1*}

1 National Institute of Immunology, New Delhi, India, **2** Department of Pharmacy, Birla Institute of Technology and Science-Pilani, Hyderabad Campus, Hyderabad, India, **3** CSIR-Institute of Genomics and Integrative Biology, New Delhi, India

* vinaykn@nii.ac.in



OPEN ACCESS

Citation: Soni V, Upadhayay S, Suryadevara P, Samla G, Singh A, Yogeewari P, et al. (2015) Depletion of *M. tuberculosis* GlmU from Infected Murine Lungs Effects the Clearance of the Pathogen. PLoS Pathog 11(10): e1005235. doi:10.1371/journal.ppat.1005235

Editor: Christopher M. Sasseti, University of Massachusetts Medical School, UNITED STATES

Received: July 2, 2015

Accepted: September 27, 2015

Published: October 21, 2015

Copyright: © 2015 Soni et al. This is an open access article distributed under the terms of the [Creative Commons Attribution License](https://creativecommons.org/licenses/by/4.0/), which permits unrestricted use, distribution, and reproduction in any medium, provided the original author and source are credited.

Data Availability Statement: All relevant data are within the paper and its Supporting Information files.

Funding: VKN received funding from Open Source Drug Discovery, CSIR OSDD/HCP0001/12FYP/2012-13/FIN/2407 and Department of Biotechnology, India BT/PR13047/Med/29/148/2009. DS received funding from Open Source Drug Discovery, CSIR OSDD/HCP0001/12FYP/2012-13/FIN/2407. VS received Senior Research Fellowship from Open Source Drug Discovery, CSIR. SU and GS are Senior Research Fellows funded by the CSIR. PS is an INSPIRE Senior Research Fellow of the Department of

Abstract

M. tuberculosis N-acetyl-glucosamine-1-phosphate uridylyltransferase (GlmU_{Mtb}) is a bi-functional enzyme engaged in the synthesis of two metabolic intermediates N-acetylglucosamine-1-phosphate (GlcNAc-1-P) and UDP-GlcNAc, catalyzed by the C- and N-terminal domains respectively. UDP-GlcNAc is a key metabolite essential for the synthesis of peptidoglycan, disaccharide linker, arabinogalactan and mycothiols. While *glmU_{Mtb}* was predicted to be an essential gene, till date the role of GlmU_{Mtb} in modulating the *in vitro* growth of *Mtb* or its role in survival of pathogen *ex vivo* / *in vivo* have not been deciphered. Here we present the results of a comprehensive study dissecting the role of GlmU_{Mtb} in arbitrating the survival of the pathogen both *in vitro* and *in vivo*. We find that absence of GlmU_{Mtb} leads to extensive perturbation of bacterial morphology and substantial reduction in cell wall thickness under normoxic as well as hypoxic conditions. Complementation studies show that the acetyl- and uridyl- transferase activities of GlmU_{Mtb} are independently essential for bacterial survival *in vitro*, and GlmU_{Mtb} is also found to be essential for mycobacterial survival in THP-1 cells as well as in guinea pigs. Depletion of GlmU_{Mtb} from infected murine lungs, four weeks post infection, led to significant reduction in the bacillary load. The administration of Oxa33, a novel oxazolidinone derivative that specifically inhibits GlmU_{Mtb}, to infected mice resulted in significant decrease in the bacillary load. Thus our study establishes GlmU_{Mtb} as a strong candidate for intervention measures against established tuberculosis infections.

Author Summary

The synthesis of the *Mtb* cell wall involves a cascade of reactions catalyzed by cytosolic and cell membrane-bound enzymes. The reaction catalyzed by GlmU_{Mtb} (an enzyme with acetyltransferase and uridylyltransferase activities) generates UDP-GlcNAc, a central nucleotide-sugar building block of the cell wall. Apart from cell wall synthesis UDP-GlcNAc is an essential metabolite participating in other cellular processes including disaccharide

Science and Technology. AS is supported by INSPIRE faculty grant IFA12-LSBM-35, from Dept of Science and Technology India. The funders had no role in the study designed, data collection, analysis, decision to publish or preparation of the manuscript.

Competing Interests: The authors have declared that no competing interests exist.

linker and mycothiol biosynthesis. GlmU_{Mtb} shares very little sequence similarity with eukaryotic acetyltransferase and uridylyltransferase enzymes. Many pathogens have alternative pathway(s) for foraging GlcNAc from the host. The present study was undertaken to see the effects of depleting GlmU_{Mtb} on pathogen survival in the host animal. We have generated a conditional gene replacement mutant of *glmU_{Mtb}* and find that depletion of GlmU_{Mtb} at any stage of bacterial growth or in mice infected with *Mtb* including a well-established infection, results in irreversible bacterial death due to perturbation of cell wall synthesis. We have developed a novel anti-GlmU_{Mtb} inhibitor (Oxa33), identified its binding site on GlmU_{Mtb}, and shown its specificity for GlmU_{Mtb}. The study demonstrates that GlmU_{Mtb} is a promising target for therapeutic intervention and Oxa33 can be pursued as a lead molecule.

Introduction

The cell wall, which contains a number of virulence determinants, is the first line of defence for survival of the pathogen in the hostile host environment [1]. The mycobacterial cell envelope includes three layers of cell membrane and a cell wall made up of peptidoglycan, mycolic acid, arabinogalactan and lipoarabinomannan (LAM) [2–4]. Most existing first line and second line drugs used to treat TB such as isoniazid, ethambutol, ethionamide and cycloserine, act on enzymes engaged in the synthesis of different cell wall components [5]. The current high mortality rates of infected individuals as well as increasing incidence of multidrug-resistant (MDR) and extensively drug-resistant (XDR) tuberculosis (TB) among patients underscore the importance of finding new targets for therapeutic intervention.

GlmU_{Mtb} is a bi-functional enzyme, with acetyltransferase and uridylyltransferase activities catalyzed by the C- and N- terminal domains respectively (Fig 1A) [6,7]. The carboxy-terminal domain of GlmU_{Mtb} transfers the acetyl moiety from acetyl CoA onto glucosamine-1-phosphate to generate N-acetylglucosamine-1-phosphate (GlcNAc-1-P). The N-terminal uridylyltransferase domain of GlmU_{Mtb} then catalyzes the transfer of UMP (from UTP) to GlcNAc-1-P to form UDP-GlcNAc (Fig 1A) [6]. The UDP-GlcNAc thus produced is among the central metabolites that is required for the synthesis of peptidoglycan, lipid A of LAM, arabinogalactan, Rha-GlcNAc linkers, mycothiol (required for maintaining redox homeostasis) [8–14]. The crystal structure of *M. tuberculosis* GlmU (GlmU_{Mtb}) displays two-domain architecture with an N-terminal α/β -like fold and a C-terminal left-handed parallel- β -helix structure [15,16]. Unlike its orthologs, GlmU_{Mtb} has a long carboxy-terminal tail which displays little secondary structure [17]. Results from transposon mutagenesis experiments have indicated *glmU_{Mtb}* to be an essential gene, supported by the fact that *M. smegmatis* is unable to grow in the absence of *glmU_{smeg}* [18–20]. However, no studies have addressed the question of whether both the activities of GlmU_{Mtb} are independently essential for the growth or survival of the bacterium.

While the enzymes required for the synthesis of UDP-GlcNAc are well conserved among prokaryotes, they are very different from those found in eukaryotes, making GlmU_{Mtb} an attractive putative drug target [21,22]. Researchers have developed compounds that inhibit the activities of the orthologs of GlmU_{Mtb} (GlmU from *T. brucei*, *P. aeruginosa*, *E. coli*, *H. influenzae* and *X. oryzae*) *in vitro* [23–30]. Bioinformatic analyses and kinetic modelling data advocate GlmU_{Mtb} to be a potential target for the development of suitable inhibitors [31]. In concurrence with these predictions, effective inhibitors have been developed against, the acetyltransferase and uridylyltransferase domains of GlmU_{Mtb} [32,33]. However, the precise sites of inhibitor-protein interactions and the efficacy of the inhibitors *ex vivo* or *in vivo* have not been

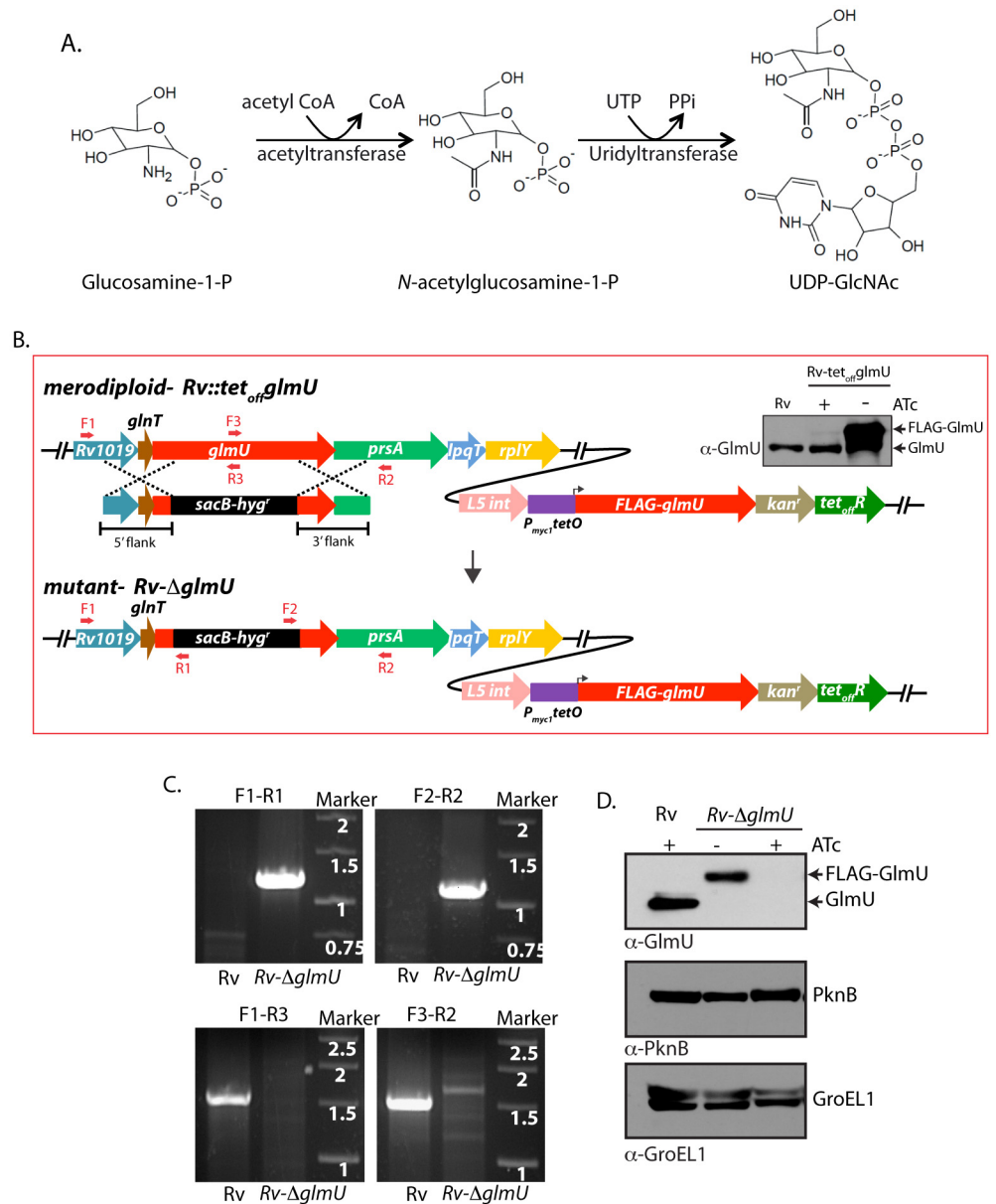


Fig 1. Generation of *glmU*_{Mtb} conditional deletion mutant. (A) Schematic depicting the biochemical reaction catalyzed by GlmU_{Mtb}. (B) Schematic diagram representing the genomic location of *glmU*_{Mtb} (*Rv1018c*) and homologous recombination between flanking sequence in the phagemid and the genomic locus. Primers used for the PCR amplification are depicted. Upper right panel shows the immunoblot. WCLs from *Rv* or *Rv::glmU* grown in the presence or absence of ATc were resolved and probed with anti-GlmU antibodies. Bands corresponding to the endogenous GlmU and ectopic FLAG-GlmU are indicated. (C) Agarose gel showing the PCR amplification of the *Rv* & putative *RvΔglmU* mutant using specific primers. Primers F1 and R2 are beyond the flanks, R1 and F2 belong to resolvase sites in *sacB/hyg^R* cassette and F3 and R3 binds to the native *glmU*. Amplification with F1-R1 or F2-R2 primers results in 1.23 kb or 1.17 kb size products with *RvΔglmU* strain but none with the *Rv*. Whereas PCRs with F1-R3 or F3-R2 primers amplifies 1.5 kb band with the *Rv* and none with the *RvΔglmU* mutant. (D) Whole cell lysates (WCL) were prepared from the large scale cultures of *Rv* and *RvΔglmU* grown in the absence and presence of ATc for five days. 20 μg of WCLs were resolved and probed with anti-GlmU_{Mtb}, anti-PknB and anti-GroEL1 antibodies. Band corresponding to endogenous GlmU_{Mtb} and FLAG-GlmU_{Mtb} are indicated.

doi:10.1371/journal.ppat.1005235.g001

investigated. Subjecting *Mtb* cultures *in vitro* to gradual decrease of oxygen (hypoxic stress) results in reprogramming of metabolic pathways and up-regulation of stress response genes, and is considered to be an *in vitro* model for the dormancy [34,35]. The importance of GlmU_{Mtb} for growth under hypoxic conditions and in an *in vivo* infection model is yet to be investigated. In the present study we have generated a conditional gene replacement mutant of *glmU*_{Mtb} and used this mutant to investigate any role GlmU_{Mtb} may play in modulating the growth of the bacterium *in vitro*, *ex vivo* and *in vivo*. The data presented here demonstrate that GlmU_{Mtb} is a viable and promising target for therapeutic intervention against tuberculosis.

Results

GlmU_{Mtb} depletion perturbs cell wall structure and affects the bacterial survival in normoxia

As the tetracycline-inducible system is an effective means to regulate gene expression [36], we introduced the integration-proficient pST-KirT-*glmU* construct (wherein *glmU*_{Mtb} gene was cloned under a promoter that shuts down upon ATc addition; S1A Fig) into *Mtb* H37Rv (Fig 1B). Whereas the expression of GlmU_{Mtb} from its native locus remained unaltered, the expression of FLAG-GlmU_{Mtb} in *Rv::glmU* strain was drastically compromised in the presence of ATc (Western blot inset, Fig 1B). This merodiploid strain was transduced with temperature sensitive phage, and the fidelity of homologous recombination at the native locus was confirmed by amplification across the replacement junctions using appropriate primers (Fig 1C). A comparison of GlmU_{Mtb} expression in the presence and absence of ATc revealed that the protein was not detectable by western blot analysis after 6 days of growth in the presence of ATc (Fig 1D). While the growth of *RvΔglmU* in the absence of ATc was similar to *Rv*, in the presence of ATc the growth was drastically compromised (Fig 2A). A comparative analysis of growth by spotting of serially diluted cultures of *Rv* and *RvΔglmU* grown in the presence versus absence of ATc showed that GlmU_{Mtb} depletion by addition of ATc led to complete inhibition of growth, with no growth detected after 6 days (Fig 2B). Interestingly, analysis of GlmU_{Mtb} expression every 24 hours post-ATc addition uncovered significant reduction in GlmU_{Mtb} expression by the third day itself (Fig 2C). These results indicate that GlmU_{Mtb} is required for the *Mtb* survival. To determine the impact of GlmU_{Mtb} depletion on cellular morphology we carried out SEM and TEM imaging analysis of *Rv* and *RvΔglmU* cells grown for three days in the absence or presence of ATc. SEM analysis revealed severe morphological perturbations in the absence of GlmU_{Mtb}, with the bacilli showing wrinkled surface and fused cells (Fig 2D). TEM analysis showed that whereas in *Rv* and *RvΔglmU* cell wall structure and thickness are comparable, there was a marked decrease in cell wall thickness in *RvΔglmU* cells where GlmU_{Mtb} was not expressed (cells grown in the presence of ATc; Fig 2E and 2F).

Impact of GlmU_{Mtb} depletion on dormant bacteria

Next we used the Wayne model to investigate the consequence of GlmU_{Mtb} depletion on the dormant bacteria under hypoxic conditions [35]. Accordingly, hypoxia was established and maintained for 42 days with depletion of GlmU_{Mtb} or addition of INH for either 22 days, or for 2 days (Fig 3A, line diagram). In agreement with previous reports, we observed that bacteria were tolerant to INH under hypoxic conditions [37] (Fig 3C), with a thicker cell wall being observed under hypoxic conditions compared with the normoxic cultures (Fig 3D and 3E). Depletion of GlmU_{Mtb} for 22 days resulted in complete clearance of growth (Fig 3B), which was also reflected in severe morphological perturbations and drastic reduction in cell wall thickness (Fig 3D and 3E). Significantly, GlmU_{Mtb} depletion for as less as 2 days decreased cell

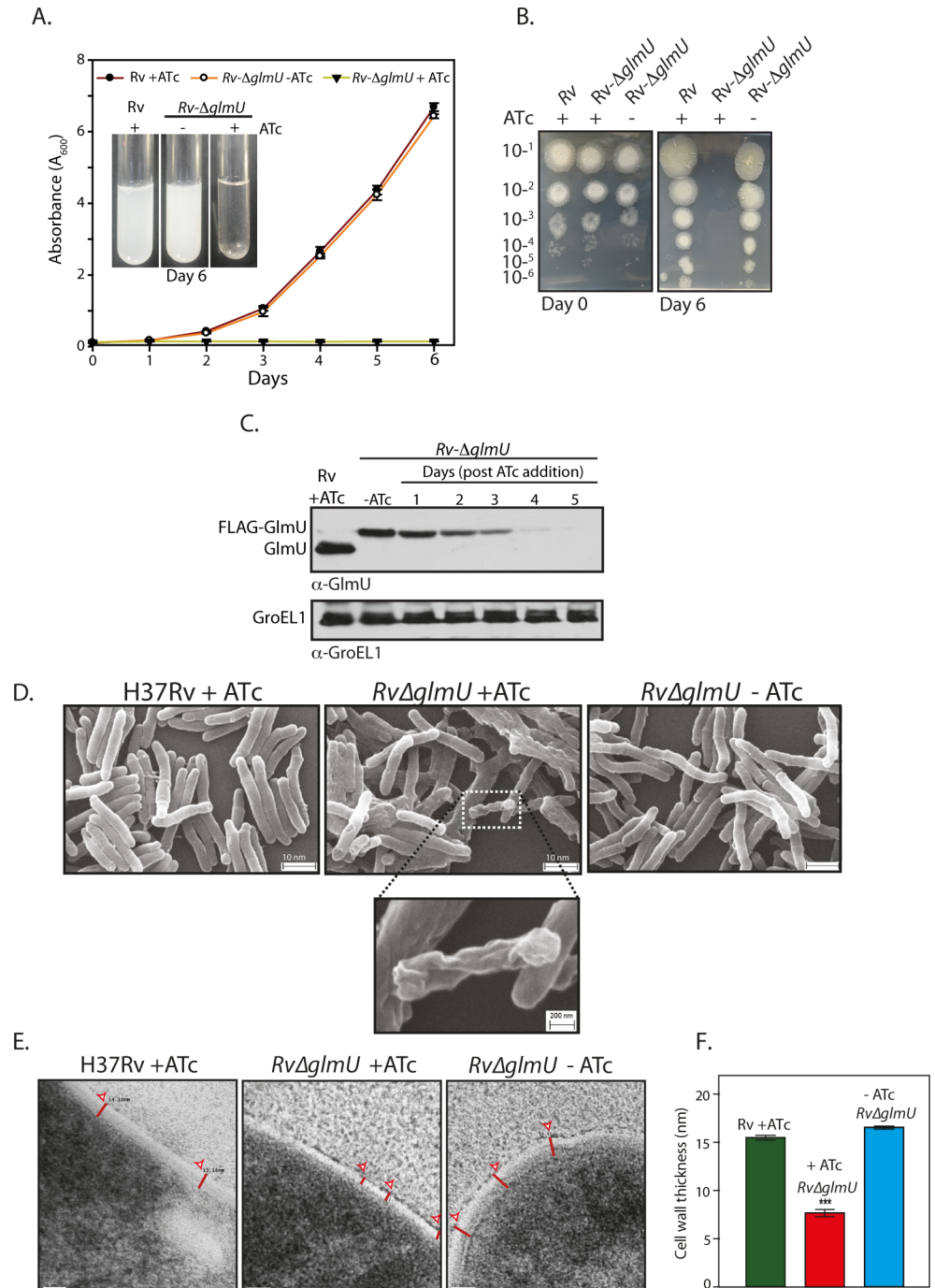


Fig 2. GlmU_{Mtb} depletion affects the bacterial survival by perturbing the cell wall structure. (A) *Rv* and *Rv Δ glmU* cultures grown to an A_{600} of 0.8 were used to seed fresh cultures at an initial A_{600} of 0.1 in the presence or absence of ATc as indicated and the day wise growth was monitored for six days. Inset shows the growth in the culture tubes after six days. The experiment was performed in triplicates ($n = 3$). Error bars indicate standard error of mean (s.e.m). **(B)** Day 0 and Day 6 cultures grown in the presence or absence of ATc were serially diluted and spotted on 7H11 agar plates. **(C)** Large scale cultures were inoculated at A_{600} of 0.1 in the presence or absence of ATc and the WCLs were prepared on different days post ATc addition (as indicated). WCLs were resolved and probed with anti-GlmU_{Mtb} and anti-GroEL1 antibodies. **(D)** Scanning electron microscopy of *Rv* and *Rv Δ glmU* grown for 72 h with or without ATc as indicated. Scale bars in upper panel were 10 nm and for the inset was 200 nm. The experiment was repeated thrice. **(E)** Transmission electron micrographs results at 50,000X of *Rv* and *Rv Δ glmU* cultures grown with or without ATc. Red lines

depict the cell wall thickness. Scale bar: 20 nm. (F) Cell wall thickness was measured in nm for 15 to 22 cells for each sample. *** $p < 0.0001$, two tailed non parametric *t*-test, mean, s.e.m.

doi:10.1371/journal.ppat.1005235.g002

viability by three orders of magnitude (Fig 3B) and decrease in cell wall thickness (~18%; Fig 3D and 3E). Taken together, the data suggests that the absence of GlmU_{Mtb} in hypoxic condition leads to aberrant cell wall thickness and morphology, eventually leading to the death of the cell.

Acetyl and uridyltransferase activities of GlmU_{Mtb} are independently essential

Biochemical investigations have shown that the N-terminal fragment (1–352 amino acids) and C-terminal fragment (150–495 amino acids) of GlmU_{Mtb} can independently undertake uridyltransferase and acetyltransferase activities respectively (Fig 4A and 4B) [15,17]. The active site residues that are necessary for these activities have also been identified (Fig 4A and 4B) [17]. To investigate if both activities are essential for cell survival, we have generated previously reported truncation mutants GlmU-N and GlmU-C [38]. We also generated GlmU_{K26A} and GlmU_{H374A}, the uridyltransferase and acetyltransferase active site mutants, and GlmU_{DM} wherein both the active site residues were concomitantly mutated. GlmU_{Mtb} wild type and mutant proteins were purified (Fig 4C) and their uridyltransferase and acetyltransferase activities were assayed. While GlmU-C and GlmU_{K26A} mutants showed acetyltransferase activity, as expected they did not show any uridyltransferase activity (Fig 4D). On the other hand GlmU-N and GlmU_{H374A} had uridyltransferase activity but not the acetyltransferase activity (Fig 4D). As expected the double mutant did not have either uridyl or acetyltransferase activity (Fig 4D). Next complementation assays using one or other truncations / active site mutants were carried out. The FLAG-GlmU_{Mtb} and the complemented untagged wt-GlmU_{Mtb} proteins were found to be expressed at similar levels (Fig 4E). The episomally expressed wt-GlmU_{Mtb} could rescue the *RvΔglmU* phenotype in the presence of ATc (Fig 4F). Contrastingly, while the various GlmU_{Mtb} mutant proteins were expressed at levels comparable to that of FLAG-GlmU_{Mtb} (Fig 4E); none of them rescued the growth defects of the *RvΔglmU* strain in the presence of ATc (Fig 4F). These results indicate that both uridyltransferase and acetyltransferase activities of GlmU_{Mtb} are essential for pathogen survival and imply that the only source of the metabolites GlcNAc-1-P and UDP-GlcNAc is through the GlmU_{Mtb} mediated synthesis pathway.

Presence of GlmU_{Mtb} is obligatory for the survival of *Mtb* in the host

Mtb cells devoid of an intact cell wall have been found to be capable of surviving inside the host [39,40]. Some pathogens have been reported to resort to cell wall “recycling” for the synthesis of UDP-GlcNAc, and others have been known to utilize GlcNAc from the host for this purpose [41–44]. However, such mechanisms have not yet been reported in *Mtb*. To investigate these possibilities we examined the impact of GlmU_{Mtb} depletion on survival of the pathogen in the host. Using an *ex vivo* THP-1 infection model we observed ~80% phagolysosome fusion in the absence of GlmU_{Mtb} (Fig 5A and 5B; compare *RvΔglmU* with *RvΔglmU* +ATc). This was also reflected in the survival pattern of the pathogen upon depletion of GlmU_{Mtb} (Fig 5C), with survival being strongly compromised in absence of GlmU_{Mtb}. The impact of GlmU_{Mtb} depletion was evident as early as 24 h post-infection, with a dramatic drop in survival by 48 hours post-infection (Fig 5C). The consequences of GlmU_{Mtb} depletion on survival of the pathogen *in vivo* were evaluated using guinea pig infection model. CFUs obtained 24 h after infection suggested

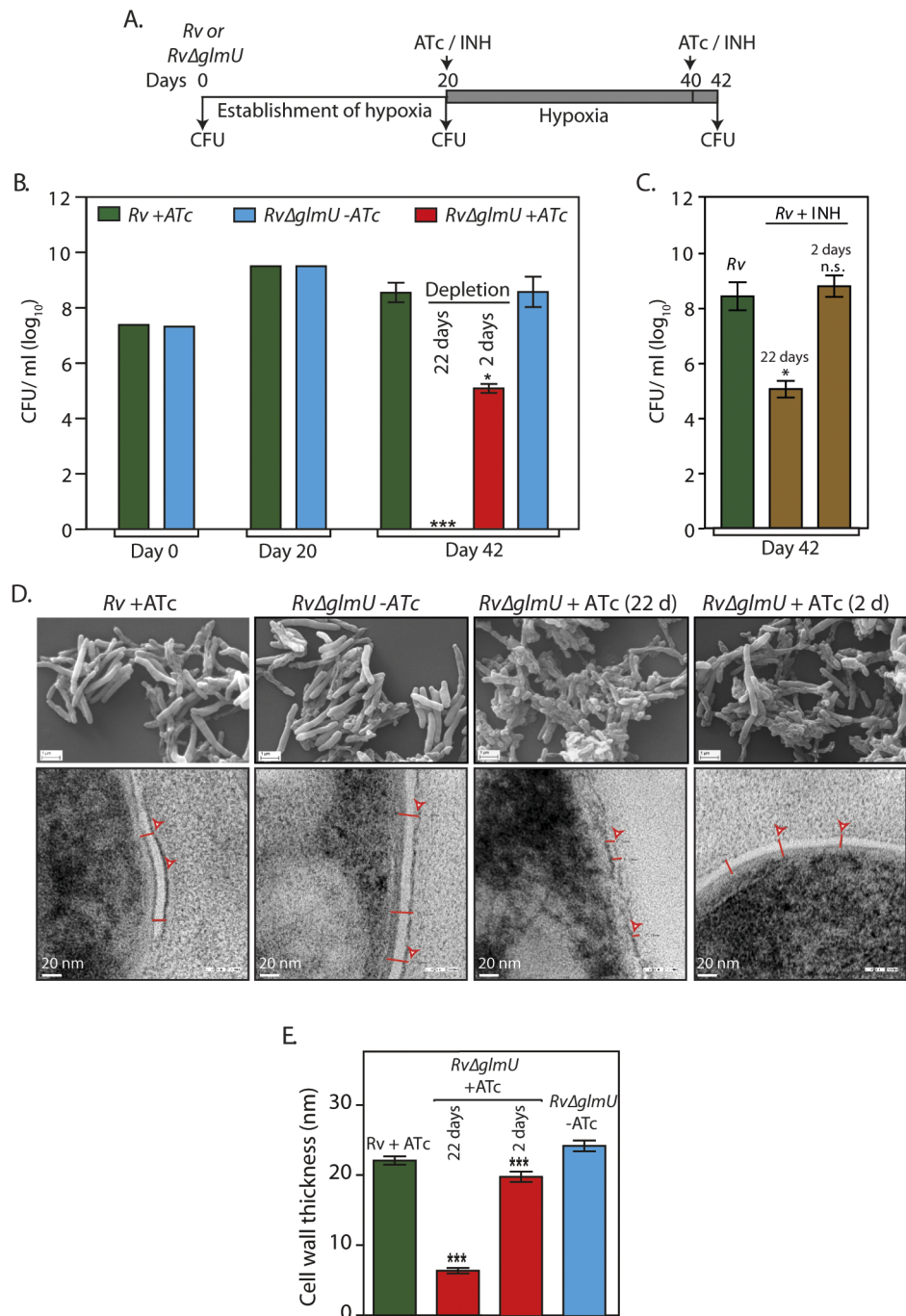


Fig 3. Effect of GlmU_{Mtb} depletion of dormant bacteria. (A) Schematic outline of the experiment. (B) *Rv* and *RvΔglmU* cultures were seeded at an initial A_{600} of 0.1 in 1.5 HPLC tubes or in 500 ml flasks containing penetrable caps. Establishment of hypoxia was monitored with the help of methylene blue color change (blue to colorless). ATc was added to *Rv* on 20th day and to *RvΔglmU* on 20th and 40th day. CFUs were enumerated on day 0, day 20 and day 42. * $p < 0.05$ or *** $p < 0.005$, two tailed non parametric *t*-test, Error bars indicate s.e.m. and the experiment was performed in triplicates ($n = 3$). (C) INH (50 ng/ml) was added to the hypoxic *Rv* cultures on 20th and 40th day. CFUs were enumerated on day 42. * $p < 0.05$ or NS: non-significant, two tailed non parametric *t*-test, Error bars indicate s.e.m. and $n = 3$. (D) Large scale hypoxic cultures were pelleted down on day 42 and processed for scanning electron microscopy (upper panel) or transmission electron microscopy (lower panel) imaging. (SEM: scale bars: 1 μ m; TEM scale bar: 20 nm). Cell wall thickness is indicated by red lines. (E) Cell wall thickness was measured in nm for 20 to 54 cells from the TEM

images of different samples (representative image shown in Fig 3C). *** $p < 0.0001$ and 0.0005 , two tailed non parametric t -test, Error bars indicate s.e.m.

doi:10.1371/journal.ppat.1005235.g003

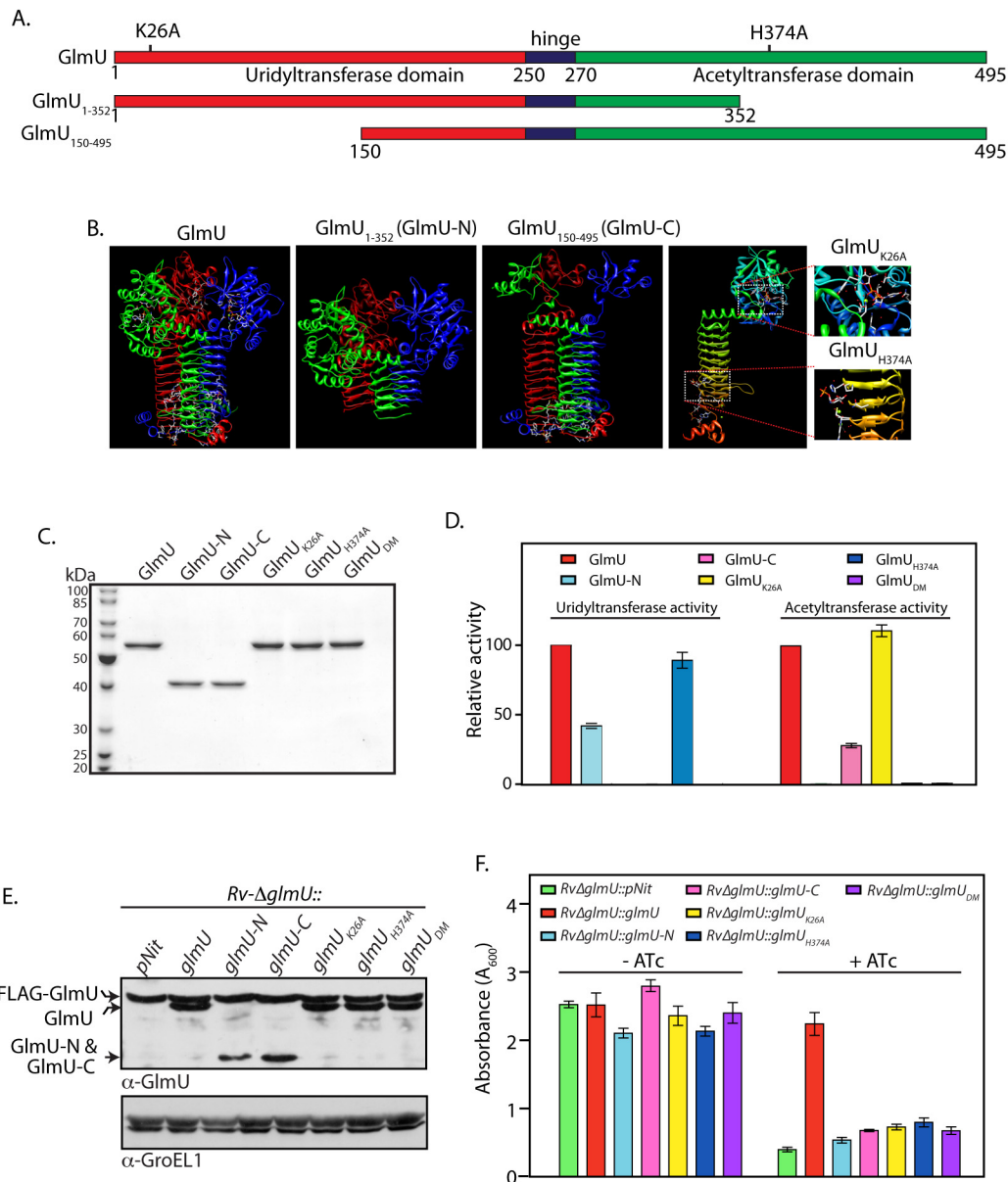


Fig 4. Acetyl and uridylyltransferase activities are independently essential. (A) and (B) Schematic and cartoon representation of GlmU_{Mtb} depicting different domains, active site residues and the deletion mutants. (C) GlmU_{Mtb} and GlmU_{Mtb}-mutants were purified as described earlier [38] and the 1 μg of the purified proteins were resolved on 10% SDS-PAGE and stained with coomassie. (D) Uridyltransferase (left panel) and acetyltransferase (right panel) activities were carried out as describe in Methods using 0.5 to 20 pmoles of wild type or mutant GlmU_{Mtb} proteins. Activity was defined as μM product formed / min / pmole of enzyme. Relative activities of the mutants were calculated with respect to the activity of GlmU_{Mtb}, which was normalized to 100%. The experiment was repeated three times and the error bars indicate s.e.m. (E) Wild type and mutated GlmU_{Mtb} genes were cloned into pNit vector without any N- or C- terminal tag. pNit-*glmU*_{wt} or pNit-*glmU*_{mutant} constructs were electroporated into *RvΔglmU*, and the WCLs prepared from *RvΔglmU* and *RvΔglmU::glmU_{mutant}* cultures were resolved and probed with anti-GlmU and anti-GroEL1 antibodies. Bands corresponding to FLAG-GlmU_{Mtb}, complemented GlmU_{wt}/mutant and the deletion fragments of GlmU are indicated. (F) *RvΔglmU* and *RvΔglmU::glmU_{mutant}* cultures were seeded at an initial A₆₀₀ of 0.1 and grown for five days in the absence or presence of ATc. The experiment was performed in triplicates and the error bars represent s.e.m.

doi:10.1371/journal.ppat.1005235.g004

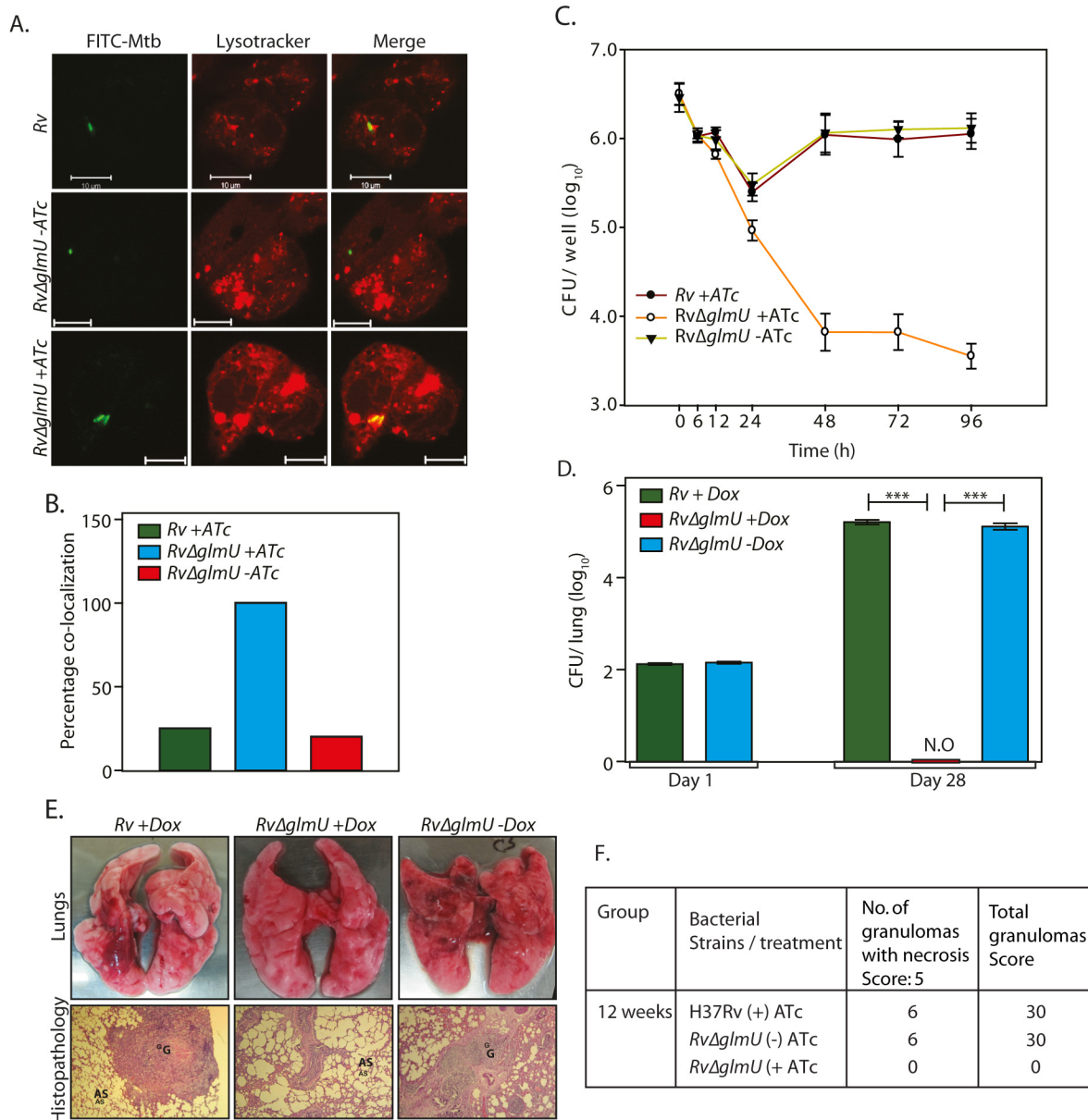


Fig 5. Presence of GlmU_{Mtb} is obligatory for the survival of Mtb in the host. (A) Confocal microscopy images of THP1 cells infected with *Rv* and *RvΔglmU* in the presence or absence of ATc as indicated were taken 48 h post infection. Bacteria were stained with FITC (green) and lysosomes were stained with Lyso Tracker red DND 99 (red). Scale bars, 10 μ m. (B) Quantification of percentage co-localization of bacterium and lysosomes in Fig 3A. n = 10 to 15. (C) PMA differentiated THP1 cells were infected with *Rv* and *RvΔglmU* and either ATc (400 ng/ml) or the vehicle were added at 0 h. CFUs were enumerated at different time points post infection. The experiment was performed in triplicates and error bars represent s.e.m. (D) Guinea pigs were infected with 150–200 bacilli CFUs of *Rv* or *RvΔglmU* and Dox was provided in the water as indicated. Guinea pigs (n = 2) were sacrificed on day 1 and homogenates from the lungs were plated in triplicates to determine the implantation. Guinea pigs (6 guinea pigs /group) were sacrificed four weeks post infection and CFUs were determined in the lung homogenates and results were plotted with log₁₀ /lung on the Y-axis and samples on the X-axis. At four weeks post infection mean CFUs for *Rv* +Dox or *RvΔglmU* +Dox and *RvΔglmU* -Dox were 5.2, 0 and 5.11 on log₁₀ scale. ****p*<0.0001, two tailed non parametric *t*-test, error bars represent s.e.m. (E) Overall pathology (upper panel) and histopathology (lower panel, HE, 40X) of the infected guinea pig lungs four weeks post infection. Both *Rv* +Dox and *RvΔglmU* -Dox were having prominent granuloma and necrotic lesions in the central and epithelioid cells and lymphocytes around it. Guinea pigs infected with *RvΔglmU* +Dox were showing normal lung parenchyma with clear alveolar spaces. G = Granuloma, AS = Alveolar Space. (F) Granuloma scores from histopathology results.

doi:10.1371/journal.ppat.1005235.g005

efficient and equivalent implantation of both wild type and mutant bacilli in the lungs of guinea pigs (Fig 5D). Discrete bacilli were observed in the lungs of guinea pigs infected with *Rv* and *RvΔglmU* 28 days post-infection (Fig 5E and 5F). In contrast, the lungs of the guinea pigs infected with *RvΔglmU* in the presence of doxycycline were clear (Fig 5E and 5F). In addition splenomegaly was significantly reduced upon depletion of GlmU_{Mtb} (*RvΔglmU* + Dox; S2A and S2B Fig). Whereas the bacillary load in the lungs and spleen of guinea pigs infected with *Rv* and *RvΔglmU* were comparable, we did not detect any bacilli when the *RvΔglmU* infected guinea pigs were administered Dox (Fig 5D). In accordance with these observations, while the gross pathology of lungs infected with *Rv* and *RvΔglmU* displayed considerable granulomatous architecture, normal lung parenchyma was observed upon GlmU_{Mtb} depletion (Fig 5E). These results suggest that the presence of GlmU_{Mtb} is obligatory for mycobacteria to survive in the host.

Depletion of GlmU_{Mtb} from infected lungs leads to clearance of pathogen

It was apparent from the data presented above that the addition of ATc or Dox at the time of inoculation or at the time of infection does not allow mycobacterial cell growth or survival in the host. In the ideal candidate for therapeutic intervention, inhibiting the activity of/ depleting the enzyme at any stage of the infection should result in pathogen clearance. We assessed this parameter of GlmU_{Mtb} by providing ATc at different stages of bacterial growth (early, log and stationary phases) and investigating its influence on cell survival in liquid cultures. Addition of ATc to *RvΔglmU* cultures on the 2nd, 4th or 6th day after inoculation significantly thwarted growth (Fig 6A). A similar analysis of bacterial growth by serial dilution of cultures followed by spotting on solid medium also revealed that viability was compromised by ~2 log fold 48 h after the addition of ATc, indicating that GlmU_{Mtb} depletion negatively impacted cell survival regardless of which stage of cell growth it was depleted at (S3A Fig).

The influence of GlmU_{Mtb} depletion on an established *ex vivo* infection was estimated by providing ATc 24 h post-infection in a THP-1 infection model. As expected the bacillary load in THP-1 cells infected with *Rv* and *RvΔglmU* were similar at 0 and 24 h after infection (Fig 6B). In contrast, while at 96 h post-infection the bacillary load for *Rv* and *RvΔglmU*- infected THP-1 cells remained the same, the addition of ATc to *RvΔglmU*- infected THP-1 cells 24 h after infection decreased the pathogen load by ~2.5 log fold, indicating that the reduction of GlmU_{Mtb} levels impacts pathogen survival even in an established *ex vivo* infection (Fig 6B). We extended this investigation to analyze the effect of GlmU_{Mtb} depletion from a fully-infected lung using murine infection model. As anticipated, the bacillary load in the lungs of mice infected with *Rv* and *RvΔglmU* were comparable both on Day 1 and on Day 28. Administration of Dox to *RvΔglmU* infected mice for the next 56 days (Day 28 to Day 84) drastically decreased the CFUs in the lungs (Fig 6C) and the pathogen was completely cleared from the spleen (S3B Fig). Unlike the lungs of mice infected with *Rv* and *RvΔglmU*, mice infected with *RvΔglmU* to whom Dox was administered displayed a total absence of lesions and granulomas in the lungs (Fig 6D and 6E). Collectively, these data suggest a fundamental role for UDP-GlcNAc, the end product of the GlmU_{Mtb}-mediated enzymatic reaction, in modulating the persistence of *Mtb* infection.

Oxa33: A novel allosteric GlmU_{Mtb} inhibitor

In addition to the acetyltransferase and uridylyltransferase active site pockets, GlmU_{Mtb} also contains an allosteric site. Binding of any suitable molecule/inhibitor to the allosteric site would prevent the conformational change essential for GlmU_{Mtb} uridylyltransferase catalytic activity. To target the allosteric site on GlmU_{Mtb} we drew on crystal structure data of *H. influenza*

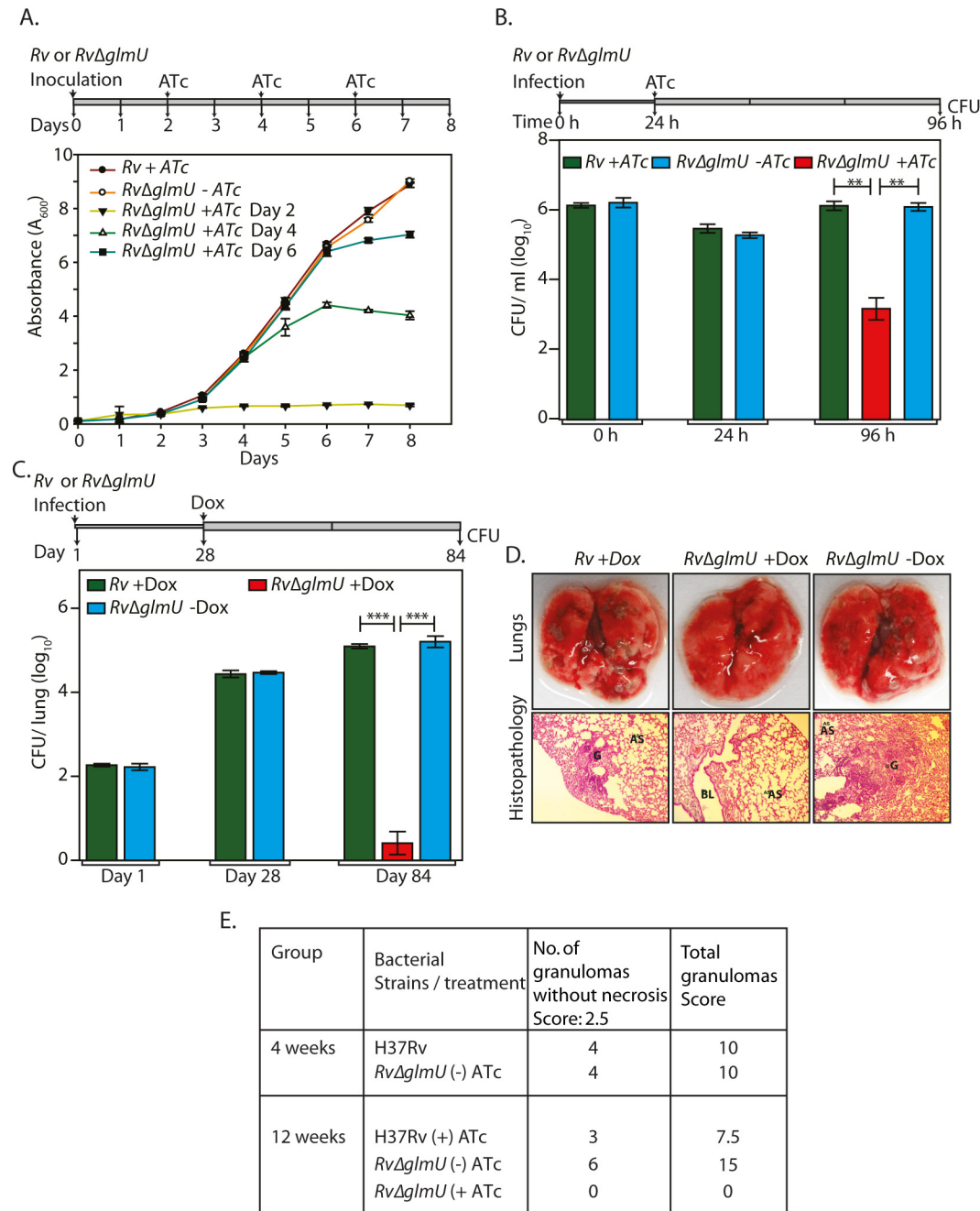


Fig 6. Depletion of GlmU_{MtB} from infected lungs leads to clearance of pathogen. (A) *Rv* and *RvΔglmU* cultures were inoculated at an initial A_{600} of 0.1 and the growth was monitored every day for eight days. ATc was added to the *Rv* culture on day 2 and *RvΔglmU* cultures were either grown in the absence of ATc or was supplemented with ATc in the growth media on 2nd, 4th or 6th day. Experiment was performed in triplicates and the error bars represent s.e.m. (B) Differentiated THP-1 cells were infected *Rv* or *RvΔglmU* cultures and the infection was allowed to be established for 24 h. 24 h post infection ATc was supplemented in the media for *Rv* and *RvΔglmU* infected cultures. As a control THP1 cells infected with *RvΔglmU* were grown without ATc. CFUs were enumerated at 0, 24 and 96 h post infection. $**p < 0.005$, two tailed non parametric *t*-test, Experiment was performed in triplicates and the error bars represent s.e.m. (C) BALB/c mice (6 to 9 mice / group) were infected with *Rv* and *RvΔglmU* strains and the infection was established for next 28 days. Subsequently, Dox was provided (with 5% dextrose on every alternate day) in the drinking water for *Rv* infected mice. One group of *RvΔglmU* infected mice were administered with Dox and other with vehicle control for the next 56 days. CFUs were enumerated on day 1, day 28 and day 84 post infection. At 28th days post infection mean CFUs for *Rv* and *RvΔglmU* infected mice were 4.43 and 4.47 on \log_{10} scale and 84th days post infection mean CFUs for *Rv* + Dox or *RvΔglmU* + Dox and *RvΔglmU* - Dox were 5.1, 0.42 and 5.2 on \log_{10} scale. $***p < 0.0005$, two tailed non parametric *t*-test, mean, error bars represent s.e.m. (D) Overall pathology and histopathology of infected BALB/c mice lungs. Infected lungs dissected on 84th day after infection from *Rv* (+Dox) and *RvΔglmU* (-Dox) infected mice shows clear lesions (upper panel) and granuloma with lymphocytes and foamy histiocytes (lower panel, HE stain, 100x) while *RvΔglmU*

(+Dox) was showing normal lung parenchyma and no granuloma. G = Granuloma, BL = Bronchial Lumen, AS = Alveolar Space. (E) Granuloma scores from 4 and 12 weeks of histopathology results.

doi:10.1371/journal.ppat.1005235.g006

GlmU (GlmU_{HI}) bound to its allosteric small molecule inhibitor (S4A and S4B Fig) [27]. Alignment of the GlmU_{Mtb} and GlmU_{HI} allosteric pocket residues suggested that the interacting residues were conserved between the two proteins (S4C and S4D Fig). The Asinex database was screened against shape as described (S5A Fig) and the resulting 43 hits were biochemically characterized for their ability to inhibit GlmU_{Mtb} uridylyltransferase activity. One of the promising molecules was used for further structural optimization (S5A Fig). Of the 53 structurally optimized compounds one molecule, namely (4Z)-4-(4-benzyloxybenzylidene)-2-(naphthalen-2-yl)-1,3-oxazol-5(4H)-one (Oxa33; Synthesis scheme provided in Figs 7A and S5B), was found to be an efficient inhibitor of GlmU_{Mtb} activity with an IC₅₀ of 9.96±1.1 μM (Fig 7B). Isothermal titration analysis suggested an adequately high affinity binding for the compound (K_a = 2.35×10⁶ M⁻¹), with a binding stoichiometry of 0.7 (S6A Fig). We sought to identify the residues in GlmU_{Mtb} that are critical for interacting with Oxa33. Docking and MD simulation studies revealed polar, non-polar and hydrophobic interactions between Oxa33 and the allosteric site residues (Figs 7C, S6B and S6C). Based on the obtained data a panel of GlmU_{Mtb} proteins each carrying a single mutation was created, the mutant proteins were purified (S6D Fig), and their uridylyltransferase activity assayed. While all the mutants had similar levels of uridylyltransferase activity there was a substantial increase in their IC₅₀ values, suggesting a loss of interaction with Oxa33 (Fig 7D and 7E).

To decipher the mechanism of Oxa33 mediated inhibition of uridylyltransferase activity, we superimposed the GlmU_{Mtb}-Oxa33 complex with the unbound GlmU_{Mtb} structure. Upon Oxa33 binding, the loop regions (in the range of 3–6 Å) at the uridylyltransferase active site undergo significant conformational changes, decreasing the active site volume, which results in occlusion of the substrates (Fig 7F). Differential scanning fluorimetry (DSF) analysis of GlmU_{Mtb} in the presence of Oxa33 showed a 3°C shift in protein melting temperature (T_m) validating the conformational changes (S5E Fig). Interestingly we also observed much higher relative fluorescence units (~10000 vs 2500) in the presence of Oxa33, which is likely due to the compound induced structural changes facilitating increased binding of the dye (S6E Fig). Together, these data demonstrate that Oxa33 binds to the allosteric site at N-terminal domain of GlmU_{Mtb} and inhibits its uridylyltransferase activity by causing structural changes.

Specificity and efficacy of Oxa33

Subsequently we investigated the ability of Oxa33 to inhibit the *in vitro* growth of *Mtb H37Rv*. Oxa33 inhibited the *in vitro* growth of *Mtb H37Rv* with a minimum inhibitory concentration (MIC) of ~75 μM (~30 μg / ml) and a maximum bacteriocidal concentration (MBC) of ~150 μM (~60 μg / ml). To ascertain if this inhibitory effect was due to inhibition of GlmU_{Mtb} activity we overexpressed GlmU_{Mtb} in the cells prior to drug treatment and determined the effect of this on the MIC value (Figs 8A and S6A). Whereas the inhibition of growth in the presence of INH was similar with or without GlmU_{Mtb} overexpression in the cells (Fig 8A, lower panel), Oxa33 failed to inhibit cell growth even at concentrations as high as 150 μM (60 μg/ ml) (Fig 8A, upper panel). Interestingly when sub lethal concentration of Oxa33 was provided, the MIC of INH decreased from 32 to 16 ng/ml (S7B Fig). The impact of Oxa33 on THP1 cells 24 h after infection with either *Rv* or *Rv::glmU_{tet-on}* was also investigated. In concurrence with the *in vitro* growth data, overexpression of GlmU_{Mtb} alleviated Oxa33-mediated clearance of *Mtb* from THP-1 cells (Figs 8B, S6D and S6E). These results suggest that the inhibition of mycobacterial growth by Oxa33 is specifically due to inhibition of endogenous GlmU_{Mtb}.

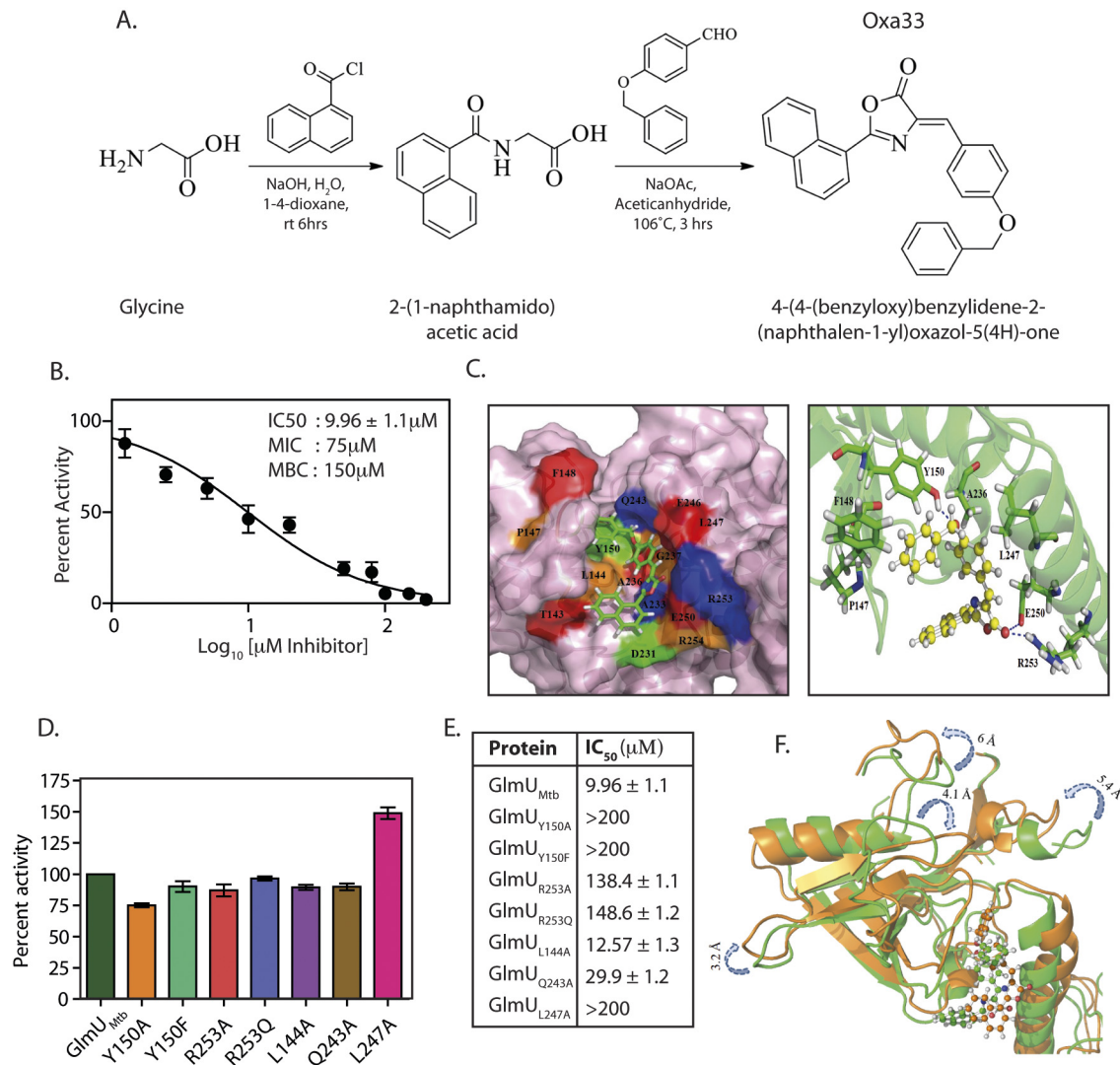


Fig 7. Oxa33, a novel inhibitor against GlmU_{Mtb} binds at allosteric site of uridylyltransferase domain. (A) Synthetic scheme for the preparation of 4-(4-(benzyloxy)benzylidene)-2-(naphthalen-1-yl)oxazol-5(4H)-one (Oxa33). (B) IC₅₀ values were determined by varying the concentration of Oxa33 and calculating the percent activity with respect to the uridylyltransferase activity of 0.75 pM conc GlmU_{Mtb} in the presence of 5% DMSO (vehicle). IC₅₀ value was calculated by plotting percentage activities against different log₁₀ values of inhibitor concentrations (µM). Experiment was performed in triplicates and the error bars represent s.e.m. (C) Left panel depicts docking surface representation of the allosteric site of the GlmU_{Mtb} allosteric site in complex with Oxa33. Right panel represents ribbon cartoon showing the amino acids residues of allosteric site and hinge region interacting with Oxa33 (in ball and stick model). Tyr150, Glu250 and Arg 253 were found to be in hydrogen bonding with carbonyl oxygen over the oxazole ring. While Leu144, Pro147, Phe148, Tyr150, Ala233, Ala236 and Leu247 participate in strong hydrophobic interactions with Oxa33. (D) Based on the data above GlmU_{Mtb} allosteric site mutants were created, proteins were purified and the uridylyltransferase activity of GlmU_{Mtb} mutants was determined. Wild type and mutant GlmU_{Mtb} proteins show almost comparable activity. (E) IC₅₀ values in µM were determined as described above for the wild type and the mutant GlmU_{Mtb} proteins. Tables shows the values obtained for wild type and mutant enzymes. Experiments were performed in triplicates and the error bars represent s.e.m. (F) Superimposed view of GlmU_{Mtb}-Oxa33 complex before (green) and after (orange) the simulation time period. Showing a partial closure of uridylyltransferase site (decreased volume) thereby making it unavailable for its substrates for catalysis.

doi:10.1371/journal.ppat.1005235.g007

Finally, we analysed the efficacy of Oxa33 in clearing bacilli from infected lungs using a murine infection model. Oxa33 compound is highly hydrophobic in nature. After trying many solvents, we could successfully resuspend it in 2.5% Tween-80. Prior to performing the experiments we examined the maximum dose tolerance and survival analysis to determine the toxicity (S8A and S8B Fig). Based on the data obtained we chose 50 mg / kg as the appropriate dose.

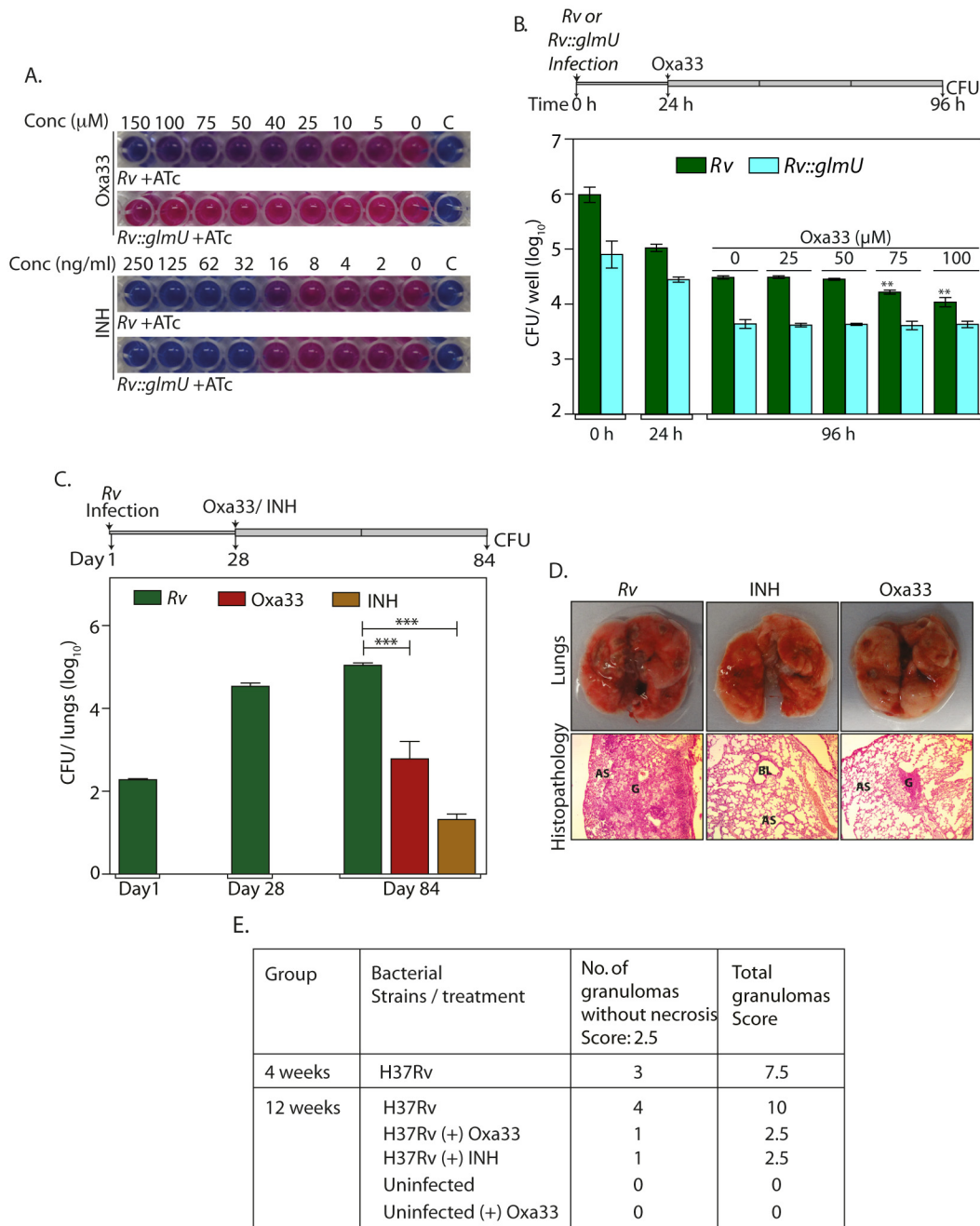


Fig 8. Specificity and efficacy of Oxa33. (A) *Rv* and *Rv::glmU_{tet-on}* cultures were grown in presence of 1 μg/ml ATc and different concentrations of Oxa33 or INH (as indicated). 0.02% resazurin dye was added on day 7. Pink colour indicates viable bacteria while blue colour indicates dead bacteria. 'C' denotes culture media control. The experiment was performed thrice. (B) Differentiated THP1 were infected either with *Rv* or *Rv::glmU_{tet-on}* and grown in RPMI media containing 400 ng/ml ATc. 24 h post infection different concentrations (as indicated) of Oxa33 or vehicle control was supplemented to the media for the next 72 h followed by CFU enumeration. Experiment was performed in triplicates and the error bars represent s.e.m. (C) BALB/c mice (7 to 11 mice / group) were infected with *Rv* and the infection was allowed to be established for 28 day. Oxa33 (50 mg/kg, intraperitoneal, in 2.5% Tween 80) or INH (25 mg/kg, in drinking water with 5% sucrose) were administered to the mice for a subsequent period of 56 days. CFU in the lungs of mice were determined on 1, 28 and 84 days post infection. Day 1st and day 28th CFUs show successful implantation and establishment of infection, respectively. 56 days of Oxa33 or INH treatment partially reduces the mean bacillary load to 2.78 and 1.3 on log₁₀ scale. ****p*<0.0005 or 0.0006, two tailed non parametric *t*-test, error bars represent s.e.m. (D) While the overall pathology of lungs (upper panel) illustrates robust Mtb infection in untreated mice, relatively smaller and fewer lesions and granulomas were observed in Oxa33 or INH treated mice. Lower panel exhibit hematoxylin and eosin stained photomicrograph of lungs from *Rv*, INH treated and Oxa33 treated mice at 100x magnification. This histopathological analysis shows large or small granuloma with lymphocytes and foamy histiocytes in *Rv* infected mice or Oxa treated mice respectively G = Granuloma, BL = Bronchial Lumen, AS = Alveolar space. (E) Granuloma scores from lungs of infected and treated mice for 4 weeks and 12 weeks.

doi:10.1371/journal.ppat.1005235.g008

Since it was difficult to predict the fate of Oxa33 during the process of digestion, we avoided using the oral administration route. We chose intra peritoneal route for administering the compound as the intravenous (I/V) injection of Tween 80 (solvent) in the animals was known to cause hypersensitivity and anaphylactic shock [45,46].

Groups of mice were infected with *Rv* and were treated with vehicle, INH, or Oxa33 at 28 days post-infection, for a duration of 56 days (Fig 8C, line diagram). Compared with the vehicle-treated group where we observed a marginal increase in bacillary load, a significant reduction in the bacillary load was observed in the lungs and spleen of both, INH- and Oxa33-treated groups (~4 and 2.5 log fold, respectively for lungs) (Figs 8C and S9A). This was also reflected in the gross pathology and histopathology of lungs (Fig 8D and 8E). Although *in vitro* MBC values of Oxa33 was ~150 μ M (60 μ g/ml), it seems to be a relatively more efficacious *in vivo*, which could be due to its accumulation in the lungs of the infected mice. To investigate this possibility uninfected mice were treated with 50 mg/kg Oxa33 for a period of 3 weeks or 8 weeks. In order to estimate the concentration of Oxa33 in the lung, we first determined the absorbance spectra for Oxa33, which gave a clear peak at 401 nm (S10A Fig). We determined the A_{401} at different concentrations of Oxa33 and the standard curve was plotted (S10B and S10C Fig). Oxa33 was extracted from the lungs and its concentration was determined. The concentrations of Oxa33 in the lungs were in the range of ~200–300 μ g/lung at 3 weeks and ~800–1300 μ g/lung at 8 weeks (S10D Fig). The accumulation of Oxa33 in the lungs is ~13 to 18 fold higher than the MBC values, which may be the reason for higher potency of Oxa33 *in vivo* compared with the *in vitro* experiments. Taken together, the results presented in this study establish GlmU_{Mtb} to be an effective target against which new sets of inhibitors may be developed.

Discussion

Cell wall provides the structural rigidity and protects bacteria from various environmental and physiological insults. Biosynthesis of the cell wall of bacteria is a complex process requiring enzymes localized to different cellular compartments [47]. Due to the essentiality of the enzymes involved they are considered attractive targets for anti-microbial therapies. The majority of the first line and second line anti-tuberculosis drugs from the existing regimen target enzymes involved in cell wall synthesis [5]. These include Isoniazid and Ethionamide targeting enoyl-[acyl-carrier-protein] reductase and inhibiting mycolic acid synthesis, Ethambutol targeting arabinosyl transferase and inhibiting arabinogalactan biosynthesis, and Cycloserine targeting D-alanine racemase and ligase, which inhibits peptidoglycan synthesis [5]. However most of these drugs are not very effective against dormant/ latent *Mtb* [48].

UDP-GlcNAc is a critical metabolite both in prokaryotes and eukaryotes. In eukaryotes it is mainly utilized for O- or N- GlcNAcylation, sialic acid biosynthesis and hylauronic acid biosynthesis [49–51]. In addition to the peptidoglycan synthesis [10], in gram negative bacteria UDP-GlcNAc is required for the synthesis Lipid A subunit of lipopolysaccharide [52] and in gram positive bacteria it is required for Rha-GlcNAc linker [53], arabinogalactan [54], teichoic acid synthesis [55]. In few prokaryotes, UDP-GlcNAc has also been shown to be required for sialic acid [56], N-GlcNAcylation [57] and poly (-GlcNAc)_n [58]. GlmU_{Mtb}, an enzyme with dual activity, synthesizes a core metabolite necessary for the synthesis of cell wall peptidoglycan, UDP-GlcNAc [6]. Interestingly, we found that depleting GlmU_{Mtb} during both normoxic and hypoxic growth resulted in substantial decrease in cell viability (Fig 3). This may be due to the requirement of UDP-GlcNAc, which in addition to participating in cell wall synthesis is also required for other cellular processes such as mycothiol biosynthesis (to maintain redox homeostasis) [14,59]. However, the TEM data clearly shows decreased cell envelop thickness

even in hypoxic conditions (Fig 3). Although the CFUs do not change significantly the cells may be undergoing significant replication, which might be balanced by death [60]. Alternatively, new cell envelop may be required even if the bacteria are not replicating. Thus one can rule out the possibility that decreased viability may well be due to requirement of UDP-GlcNAc for the cell envelop synthesis.

While UDP-GlcNAc is a critical metabolite for both prokaryotes and eukaryotes, the enzymes involved in its *de novo* synthesis are significantly different [10]. In addition, both prokaryotes and eukaryotes can utilize GlcNAc from different sources to synthesize UDP-GlcNAc through salvage pathways [61–63] (S11 Fig). *Capnocytophaga canimorsus*, a member bacteria from Bacteroidetes phylum lacks endogenous GlmM and GlmU required for the synthesis of GlcNAc and it instead relies on GlcNAc obtained from forages glycans from the host mucin and N-linked glycoproteins [42]. Depending on the enzymes of the salvage pathway present in the bacterial system, it would require either both the activities or only the uridyltransferase activity of GlmU_{Mtb} for UDP-GlcNAc synthesis. Till date the presence of alternate salvage pathway in *Mtb* has not been demonstrated. However, even with an operating salvage pathway GlmU_{Mtb} is essential for the utilization of host GlcNAc to form UDP-GlcNAc (S11 Fig). In line with this, we find that depletion of GlmU_{Mtb} during *ex vivo* or *in vivo* infection either at the start or after infection has been definitively established leads to clearance of pathogen.

GlmU_{Mtb} and the acetyltransferase and uridyltransferase enzymes found in eukaryotes share very little sequence similarity. Although efforts have been made by different groups to target bacterial GlmU proteins, the specificity of these inhibitors for GlmU *in vivo* have not been established [23–30]. Most GlmU inhibitors characterized till date target either the acetyl- or uridyltransferase active sites. In contrast, inhibitors of GlmU_{HI} target the allosteric site near the uridyltransferase active site [27]. The interaction of the inhibitor with the enzyme via this allosteric site perturbs the active site conformation of the protein, thus inhibiting uridyltransferase activity [27]. In the present study we have used shape based designing and developed a novel oxazolidine molecule, Oxa33, and characterized its ability to bind to the GlmU_{Mtb} allosteric site. MD simulation and mutation of critical interacting residues to defined the possible allosteric site residues required for Oxa33 binding (Fig 7). DSF (S6E Fig) and structural superimposition (Fig 7) supports that inhibition of uridyltransferase activity is due to structural changes in the N-terminal domain of GlmU_{Mtb}. Further in order to determine the specificity of Oxa33, GlmU_{Mtb} over expressing strains of *Rv* was used to determine the MIC. Both *in vitro* and *ex vivo* results (increased MIC or MBC) validate that Oxa33 specifically binds to GlmU_{Mtb} inside the bacteria. Administrating the Oxa33 to fully infected (28 days) mice resulted in partial ablation of pathogen load in the lungs. Taken together results presented here demonstrates that GlmU_{Mtb} is a viable and promising target for therapeutic intervention and Oxa33 can be pursued as a lead molecule, which needs to be developed further to improve its efficacy.

Materials and Methods

Chemicals and reagents

Restriction enzymes and Phu DNA polymerase were purchased from New England Biolabs. pENTR/directional TOPO cloning kit (Invitrogen), pQE2 (Qiagen), were procured from the respective sources. Analytical grade chemicals and oligonucleotide primers were procured from Sigma. Malachite green phosphate assay kit (POMG-25H) was purchased from BioAssay System (Gentaur). Electron microscopy reagents were purchased from Electron Microscopy Sciences. Media components were purchased from BD Biosciences. Doxycycline hydrochloride was purchased from Biochem pharmaceutical.

Generation of *glmU* conditional gene mutant in *M. tuberculosis*

The hexa-His tag in the pST-KiT construct [15] was replaced with an N-terminal FLAG tag, and the tetracycline repressor gene (*tetR*) was replaced with a reverse *tetR* (*r-tetR*) from pTC28S15-OX [64] to create plasmid pST-KiT. To generate the integrating shuttle plasmid pST-KiT-*glmU*_{Mtb}, the *glmU*_{Mtb} gene was excised from pQE2-*glmU*_{Mtb} using *NdeI-HindIII* digestion and was subcloned into the corresponding sites on pST-KiT. The resulting pST-KiT-*glmU* construct expresses GlmU_{Mtb} in the absence of inducer ATc. Upon addition of ATc, ATc binds to the r-TetR repressor resulting in the conformational change that would allow it to bind to the operator sequences in P_{myc}tetO (S1 Fig) [64]. The integration-proficient plasmid containing the inducible *glmU*_{Mtb} gene was electroporated into mycobacterial cells to create the merodiploid strain *Rv::glmU*_{Mtb}. 5' and 3' genomic flank sequences of *glmU*_{Mtb} (approximately 1 kb on either side) were amplified, the amplicons digested with *PflMI*, and ligated with the antibiotic resistance cassette along with the *oriE* and *cosλ* fragments generated from pYUB1474 construct, to generate the allelic exchange substrate (AES) [65]. The AES was linearized using the unique *PacI* site and then cloned into temperature sensitive shuttle phagemid phAE159 at the *PacI* site. A conditional gene replacement mutant of *RvΔglmU* was created from the merodiploids with the help of specialized transduction methodology (S1A Fig) [66]. *RvΔglmU* recombinants obtained were analyzed by PCR amplification to verify the fidelity of the recombination event.

Analysis of growth patterns

H37Rv (*Rv*) and *RvΔglmU* cultures were grown in Middlebrook 7H9 medium supplemented with 10% ADC (albumin, dextrose and catalase), or in 7H11 medium supplemented with 10% OADC (oleic acid, ADC). To analyze bacterial growth *in vitro*, *Rv* and *RvΔglmU* mutant bacterial cultures were inoculated at A₆₀₀ of 0.1, in the presence or absence of anhydrotetracycline (ATc), and A₆₀₀ was measured every 24 h for 6 or 8 days. For spotting analysis, cells were harvested by centrifugation, washed twice with PBST (0.05% Tween 80) to remove ATc, resuspended in 7H9 medium, and serially diluted in the same medium, followed by spotting 10 μl aliquots of the various cell dilutions on 7H11 agar plates to assess cell viability. To determine the impact of GlmU_{Mtb} depletion during hypoxia in *Rv* and *RvΔglmU* strains, we established hypoxia in 1.5 ml HPLC tubes or 500 ml flasks with penetrable caps, following modified Wayne model [35]. ATc (2 μg/ml) or isoniazid (INH) (50 ng/ml) were injected into the cultures at different time points and the number of CFUs were determined after 42 days. Scanning and transmission electron microscopy (SEM & TEM) analysis of *Rv* and *RvΔglmU* mutant grown in the presence or absence of ATc were performed as described earlier [67]. Transmission electron microscopy was performed using standard protocols. Briefly, bacteria was fixed in 2.5% glutaraldehyde and 4% paraformaldehyde, dehydrated in graded series of alcohol and embedded in Epon 812 resin. Ultrathin sections were cut and stained with uranyl acetate and lead citrate [68]. SEM images were procured using Carl Zeiss Evo LS scanning electron microscope, and TEM images were captured using Tecnai G2 20 twin (FEI) transmission electron microscope.

Generation of *glmU*_{Mtb} mutant constructs and western blotting analysis

Site directed mutations of *glmU*_{Mtb} were generated with the help of overlapping PCR and the amplicons were cloned into *NdeI-HindIII* sites of pQE-2, pNit and pST-KT vectors [15,69]. The tetracyclin repressor (TetR) expressed from the plasmids binds to the operator sequence in the promoter P_{myc}tetO in the absence of ATc (S1B Fig) [70]. Addition of ATc to TetR alleviates the repression thus inducing the expression of GlmU. pST-KT-*glmU* was electroporated into

Rv to generate *Rv::glmU_{tet-on}* strain. pNit-*glmU* (wild type and mutated) constructs were electroporated into *RvΔglmU* to generate *RvΔglmU::glmU_{wt/mutant}* strains. *Rv* and *RvΔglmU::glmU_{wt/mutant}* strains were grown in the presence or absence of ATc as described above. GlmU_{Mtb} was expressed and purified using plasmid pQE2-GlmU_{Mtb}, as described earlier [15]. Whole cell lysates (WCL) isolated from *Rv*, *RvΔglmU* and *RvΔglmU::glmU_{wt/mutant}* strains that had been grown for 5 days in presence or absence of Atc, were resolved on 10% SDS-PAGE, transferred to nitrocellulose membrane, and probed with anti-GlmU_{Mtb} and anti-GroEL1 antibodies as described earlier [15,67].

Ex vivo and in vivo infections

THP1 infection experiments were carried out with either unlabelled or FITC-labelled *Rv* and *RvΔglmU* strains at 1:10 MOI, as described earlier [71]. For examination of cells under a fluorescence microscope, infected cells (48 h post-infection) were labelled with Lyso Tracker red DND 99 dye (50 nM) and mounted with Antifade (Invitrogen) mounting agent. To determine CFUs per infected cell, the infected cells were lysed in PBS containing 0.1% TritonX-100 for 15 min and different dilutions were plated on OADC-containing 7H11 agar plates. For animal infection experiments, *Rv* and *RvΔglmU* strains grown till A₆₀₀ of 0.6 were used to infect 3 to 4 week old guinea pigs or ~ 2 month old mice as described previously [72,73]. We initially used guinea pig model system as it has robust immune response. However, for the remaining experiments we chose to use Balb/C mice model of infection as the cost associated with performing the experiments and the amount of Oxa33 required for guinea pig experiments was prohibitive. To determine the implantation dosage, the bacillary load in the lungs of guinea pigs or mice was determined 24 h post-infection. To investigate the impact of *glmU_{Mtb}* depletion on survival of the pathogen, doxycycline hydrochloride (Dox, 1 mg/ kg with 5% dextrose in drinking water) was provided to *Rv* and *RvΔglmU*-infected animals as indicated, either from the time of the infection (guinea pig experiment), or 4 weeks post-infection (mice infection experiments). To assess the impact of INH or Oxa33 treatment on pathogen survival, *Rv*-infected mice (4 weeks post-infection) were supplied with INH (25 mg/ kg body weight, with 5% dextrose in drinking water) or Oxa33 (50 mg/ kg body weight, with 2.5% Tween 80, injected intra peritoneally) every third day for 8 weeks. Bacillary loads in the lungs and spleens of infected guinea pigs and mice were determined 4 weeks and 12 weeks post-infection. Histopathological evaluation of the harvested organs was performed as described earlier [67,72,73].

Shape based screening and molecular docking studies

ROCS (Rapid Overlay of Chemical Structures), a shape based technique for rapid similarity analysis was used to assess the compounds. Gaussians and shape tanimoto were used to assess the volume and shape overlaps of the compounds, respectively. As the chemical functionality is critical, the chemical feature based similarity was also considered using ROCS colour score whose force field was composed of SMARTS patterns of the chemical functions [74,75]. The shape tanimoto score and scaled color score were considered during the selection of the compounds for further virtual screening. The compounds selected were subjected to molecular docking studies using Glide v5.8 of Schrödinger molecular modelling suite 2012 (Glide v5.8, Schrödinger). The compounds were subjected to a series of docking protocols—high throughput virtual screening (HTVS), standard precision (SP) and extra precision (XP) docking. As the docking progresses from HTVS to XP, the algorithm differs, which starts from a simple docking of compounds and ends with docking protocol with high precision and parameterization while cutting off the number of compounds.

Synthesis of 4-(4-(benzyloxy)benzylidene)-2-(naphthalen-1-yl)oxazol-5(4H)-one

To the glycine solution (3.0 g, 39.89 mmol) in water under constant stirring at 0°C, NaOH (3.19 g, 79.78 mmol) was added. This was followed few minutes later by the addition of 1-naphthoyl chloride (7.20 mL, 47.86 mmol) in 1, 4-Dioxane (20 ml) and the contents were stirred at room temperature for 6 h. The reaction mixture was concentrated to half the volume and 60 ml EtOAc was added. The EtOAc layer was washed with sat NaHCO₃ (2 × 30 mL) followed by H₂O (2 × 20 mL). The separated organic layer was dried and concentrated over anhydro Na₂SO₄ to obtain solid compound, which was washed with hexanes to get 2-(1-naphthamido) acetic acid (8.30 g, 90%) as a white solid (M.P. 152°C¹). 2-(1-naphthamido) acetic acid (2.0 g, 8.73 mmol), NaOAc (0.21 g, 2.62 mmol) and 4-benzyloxybenzaldehyde (1.85 g, 8.73 mmol) were taken in acetic anhydride and heated at 106°C for 3 h. The solid formed were filtered and washed with water to remove traces of acetic anhydride, and ethanol to remove unreacted aldehyde and other organic impurities. Final compound 4-(4-(benzyloxy)benzylidene)-2-(naphthalen-1-yl)oxazol-5(4H)-one (Oxa33; 3.14 g, 88%), purified as a yellow solid, was confirmed with nuclear magnetic resonance (NMR) [76].

Isothermal titration calorimetry

To investigate the binding of Oxa33 to GlmU_{Mtb}, we performed Isothermal Titration Calorimetry (MicroCal 2000 VP-ITC, GE Healthcare) [28]. Oxa33 was re-suspended in dialysis buffer (25 mM Tris pH 7.4, NaCl 140 mM and 15% glycerol), 100 μM of MgCl₂ containing 2% DMSO. 625 μM of Oxa33 was injected for titrations from syringe (rotating at 307 rpm) into ITC cell containing 25 μM of GlmU or blank buffer at 25°C. Each injection lasted for 20 sec with 300 sec interval between every step. The quantity of heat associated by every injection was calculated by combining the area beneath every heat burst curve (microcalories/second vs. seconds). Data was corrected for the buffer signal and fitting was done by one-site binding model. Origin software (version 7.0) was used to obtain different thermodynamic binding parameters.

In vitro cytotoxicity

Oxa33 was evaluated for its cytotoxic activity in THP1 cells with the help of alamar blue assay. Serially diluted inhibitors (in 2.5% DMSO) incubated with 5 × 10³ differentiated THP-1 cells in 96 well plates for 3 days. After 3 days cells were incubated for 5 h with 10 μl of alamar blue and color development was measured using micro-plate reader at 570 nm.

Docking and molecular dynamics simulations studies of GlmU_{Mtb} with Oxa33

Molecular dynamics (MD) simulation for the protein-ligand complex was carried out for a time scale of 20 ns so as to analyze the stability of molecular interactions between ligand and protein employing Newton's Laws of Motions. Desmond molecular dynamics system v3.1 was used for carrying out the simulations employing OPLS-AA force field [77]. The protein-ligand complex was solvated using TIP3P water model which was setup as an orthorhombic solvent box, keeping a cut-off of 10 Å from any solute atom in all directions [78]. Na⁺ counter ions were added in order to neutralize the system. A cut-off of 14 Å was maintained for calculating the solvent-solvent and solute-solvent non-bonded interactions. Initially, the system was minimized keeping the convergence threshold criteria of 1.0 kcal.mol⁻¹.Å⁻¹ so as to allow the adjustment of atoms to the system environment. A simulation for each system was performed using isothermal-isobaric ensemble (NPT) including a relaxation process. Under NPT, the system

was simulated for 12 ps using a Berendsen thermostat and a Berendsen barostat with temperature of 10K and a pressure of 1 atm. The later step of relaxation protocol included the simulation of the system for 24 ps with a temperature of 300 K and 1 atm pressure with and without restraints on solute heavy atoms. M-SHAKE algorithm was used with an integration time step of 2 fs for rearranging the hydrogen bonds in the simulation [79]. The temperature and pressure of the system were maintained at 300 K and 1.013 atm respectively. The molecular dynamics simulation was run for 20 ns recording the trajectory frames at an interval of every 4.8 ps and the trajectory analysis was carried out using the Simulation Event Analysis of Desmond.

Determination of percentage inhibition, IC₅₀ and MIC

Uridyltransferase assays were performed using malachite green phosphate detection kit as described previously [17]. Acetyltransferase activity of GlmU_{Mtb} was carried out in the presence of 500 μM each of GlcN-1-P and acetyl-CoA in a 30 μl reaction volume for 30 min at 30°C as described earlier [80]. To determine the percent inhibition by different compounds the enzyme was preincubated with either 5% DMSO or 100 μM compounds for 30 min prior to performing uridyltransferase activity assays. In order to determine the IC₅₀ values, GlmU_{wt}/mutant proteins were preincubated with different concentrations of Oxa33 compound for 30 min followed by the uridyltransferase assay. To determine minimum inhibitory concentration (MIC), 5x10⁵ bacteria of *Rv* or *Rv::glmU_{tet-on}* (overexpressing GlmU_{Mtb}) cultures (grown in the presence or absence of 2 μg/ml ATc) were mixed with 100 μl of 2.5% DMSO or different concentrations of Oxa33/ INH in 96-well plates, and incubated at 37°C for 6 days. After 6 days, 40 μl of resazurin dye (0.02% in 5% Tween-80) was added to each well and the colour change was observed after 12 h.

Ethical statement

Experimental protocol for the animal experiments was approved by the Institutional Animal Ethics Committee of National Institute of Immunology, New Delhi, India (the approval number is IAEC# 315/13). The approval is as per the guidelines issued by Committee for the Purpose of Control and Supervision of Experiments on Animals (CPCSEA), Govt. of India.

Statistical analysis

Student's *t*-test (two tailed non parametric) was used to analyze the significance of cell wall thickness, THP1 and animal infection experimental results. SigmaPlot version 10.0 and Graph-Pad Prism version 5.0 was used for the statistical analysis and for plotting the results.

Supporting Information

S1 Text. Supplementary Methods and Results. Designing and development of allosteric site inhibitors of GlmU_{Mtb}. Screening of inhibitors. Isothermal Titration Calorimetry. Docking and molecular dynamics simulations. H-bond analysis. Survival curve and maximum dose tolerance. Estimation of Oxa33 from treated mice lungs.

(DOC)

S1 Fig. Schematic representing regulation of Tet-off (A) and Tet-on systems (B).

(TIF)

S2 Fig. Effect of GlmU_{Mtb} depletion on spleen during guinea pig infection. Guinea pigs (six per group) were infected with *Rv* or *RvΔglmU* and Dox was provided in the water as indicated in Fig 5. (A) Overall pathology of the infected spleens from the guinea pigs 4 weeks post

infection. (B) CFU data from guinea pig spleens. *** $p < 0.0001$ or, two tailed non parametric t -test, mean, error bars indicate s.e.m.

(TIF)

S3 Fig. Depletion of GlmU_{Mtb} from infected spleen or any stage of growth leads to clearance of pathogen.

(A) *Rv* and *RvΔglmU* cultures were inoculated at an initial A_{600} of 0.1. ATc was added to the *Rv* culture on day 1 (a) and *RvΔglmU* cultures were either grown in the absence of ATc or was supplemented with ATc in the growth media on 1st (a), 3rd (b) or 5th (c) day. Serially diluted cultures were spotted on 7H11 agar plates after day 1, 3, 5 and 7. The experiment was performed in triplicates. (B) BALB/c mice (6 to 9 / group) were infected with *Rv* and *RvΔglmU* strains. 28 days post infection Dox was provided for *Rv* and *RvΔglmU* infected mice and one group of *RvΔglmU* infected mice were administered with the vehicle control for the next 56 days. CFUs were enumerated from the spleens of infected mice on day 28 and day 84 post infection. At 28 days post infection mean CFUs for the spleens of *Rv* and *RvΔglmU* infected mice were 2.9 and 3.15 on log₁₀ scale and 84 days post infection mean CFUs for *Rv* +Dox or *RvΔglmU* +Dox and *RvΔglmU*-Dox infected spleens were 3.67, 0 and 3.5 on log₁₀ scale. *** $p < 0.0005$, two tailed non parametric t -test, error bars indicate s.e.m.

(TIF)

S4 Fig. Structural comparison of *H. influenzae* and *Mtb* allosteric site.

(A) Surface representation of GlmU_{HI} wherein its allosteric residues are highlighted. The allosteric site of GlmU_{HI}, comprises of highly lipophilic surface and a distal depression surface. (B) Interaction of GlmU_{HI} allosteric inhibitor at the allosteric site. Hydrophobic residues are coloured in green, polar residues in blue, negatively charged residues in red. Hydrogen bond interaction of the ligand with Gln231 is shown in pink color; Glu224 is also involved in the hydrogen bonding which is not represented here. Leu133, Tyr139, Met221, Leu235 were found to be involved in strong hydrophobic interactions with the inhibitor. Interactions were plotted with LIGPLOT. (C) Sequence alignment of GlmU_{HI} and GlmU_{Mtb} allosteric site residues. Conserved residues are highlighted in red boxes. (D) Table displaying allosteric residues of GlmU_{HI} and GlmU_{Mtb}. Some of the critical residues such as Tyr150, Gln243 and Leu247 of GlmU_{Mtb} are seen to be conserved.

(TIF)

S5 Fig. Design, development and synthesis of anti-GlmU_{Mtb} inhibitor.

(A) Virtual screening workflow used towards the identification of allosteric inhibitors for GlmU_{Mtb}. Shape model of allosteric inhibitor of GlmU_{HI} was generated using ROCS software. In the initial set of screening, a total of 43 compounds were identified and tested for their ability to inhibit uridylyltransferase reaction. 10 among the 43 compounds showed ~90% inhibition at 100 μM. Of these, an oxazolone derivative was identified and further chemically derivatized to a library of 52 compounds. One compound from these, Oxa33, which showed ~90% inhibition was considered for further studies. (B) Nuclear magnetic resonance spectra of purified Oxa33 (Yellow solid). ¹H NMR (400 MHz, CDCl₃): δ 9.51 (d, $J = 8.8$ Hz, 1H), 8.38 (d, $J = 8.8$ Hz, 1H), 8.25 (d, $J = 8.4$ Hz, 2H), 8.10 (d, $J = 8.4$ Hz, 1H), 7.93 (d, $J = 8.0$ Hz, 1H), 7.74 (t, $J = 8.0$ Hz, 1H), 7.68–7.56 (m, 2H), 7.49–7.33 (m, 5H), 7.29 (s, 1H), 7.12 (d, $J = 8.4$ Hz, 2H), 5.15 (s, 2H). Anal calcd for: C₂₇H₁₉NO₃: C, 79.98; H, 4.72; N, 3.45% Found C, 79.92; H, 4.83; N, 3.54%.

(TIF)

S6 Fig. ITC, MD simulation and DSF studies of Oxa33.

(A) Isothermal titration calorimetry results of Oxa33 with GlmU_{Mtb}. Released heat increased over the period of time (μcal/sec) is presented in upper panel while corresponding binding isotherm (fitted for one site) presented in lower panel. (B) rmsd plot for GlmU_{Mtb}-oxa33 complex simulated for a period of 20ns. The complex was found to be unstable during the initial time period which can be owed for its

relaxation. After 8 ns, the complex was observed to be stable indicating the strong binding affinity of Oxa33 towards GlmU_{Mtb} (C) Hydrogen bond analysis of Oxa33 analyzed during the simulation time period. (D) Purified GlmU_{Mtb} mutants (single band) specified by the docking studies of Oxa33. (E) Differential Scanning Fluorimetry (DSF; performed in triplicates) results of Oxa33 with GlmU_{Mtb}. Left panel representing melting curve of GlmU_{Mtb} in presence of 5% DMSO. While right graph is showing -3°C T_m shift upon Oxa33 incubation with GlmU_{Mtb} protein. (TIF)

S7 Fig. GlmU_{Mtb} overexpression, cytotoxicity and effect of INH upon Rv or overexpressing strains. (A) *Rv* and *Rv::glmU_{tet-on}* strains were inoculated at an initial A₆₀₀ of 0.1 in the presence of ATc (2 µg/ml) and grown up to 5 days. WCLs were resolved and probed with anti-GlmU and anti-GroEL1 antibodies. (B) *Rv* culture was treated with sub lethal dose of Oxa33 (40 µM) and variable concentrations of INH for 6 days followed by resazurine addition. Results show decrease in MICs of INH from 32 ng/ml to 16 ng/ml. The experiment was performed in triplicates. (C) Bar graph presents the cytotoxicity of the Oxa33 on THP1 cells during the 3 days of treatment. Cell viability was checked with alamar blue based assay and absorbance at 570 nm was plotted with increasing concentrations of Oxa33 inhibitor. The experiment was performed in triplicates and the error bars represent s.e.m. (D) CFUs count results of THP1 cells infected with *Rv* (for 24 h post infection) followed by treatment with various concentrations of INH (in water) for 3 days. CFU (log₁₀) per well shows gradual increase in bacterial death with increasing INH doses. ***p*<0.005, two tailed non parametric *t*-test, mean, s.e.m., n = 3). (E) Graph illustrate CFU numbers from fully infected THP1 cells (24 h) with *Rv::glmU_{tet-on}*. Abundant GlmU_{Mtb} expression in *Rv::glmU_{tet-on}* infected THP1 cells (with ATc) does not affect INH efficacy, which gives similar results as *Rv*. ***p*<0.005, two tailed non parametric *t*-test., error bars represent s.e.m. (TIF)

S8 Fig. Dose tolerance and mice survival curves. (A) Maximum dose tolerance graph showing relative change in body weight of mice (4 mice / group) during the course of Oxa33 administration for 30 days. (B) Survival curve of mice (4 mice / group) treated with different concentrations of Oxa33 for 30 days. (TIF)

S9 Fig. In-vivo efficacy on *Mtb* load in infected mice spleen and toxicity of Oxa33. (A) *Mtb* bacterial load in the spleen of totally infected mice (7 to 11 mice /group) (for 28 days) and treated with Oxa33 or INH for subsequently 56 days. ****p*<0.0007 or ***p*<0.002, two tailed non parametric *t*-test, the error bars represent s.e.m. (B) High power (400x) photomicrograph of hematoxylin and eosin stained spleen, brain, heart, liver and lungs of untreated mice or mice treated with Oxa33 for 8 weeks. Spleen is showing usual parenchyma. WP = White Pulp, RP = Red Pulp. While, section from hippocampal area of brain showing several degenerated neuron in the neuronal layer. Section of heart is showing normal cardiac muscle fibres. Photomicrograph of liver depicts typical hepatic parenchyma. PV = Portal Vein, BD = Bile Duct. Lung section also represents usual lung parenchyma. BL = Bronchial Lumen, AS = Alveolar space. (TIF)

S10 Fig. Standard curve for Oxa33 and its estimation in treated mice lungs. (A) Absorbance spectra of Oxa33 resuspended in tetrahydrofuran (THF). It showed a peak at 401 nm. (B) Absorbance readings (401 nm; performed in triplicates; A, B and C) of Oxa33 at different concentrations (C) Standard curve of Oxa33 showing linear regression with a slope of 0.0497 OD /

µg. (D) Table showing Oxa33 concentrations (µg/lung) in the lungs of mice treated with 50 mg/kg (body weight) for 3 or 8 weeks.

(TIF)

S11 Fig. Model for the UDP-GlcNAc synthesis pathways in *Mtb*. Model shows De novo pathway for UDP-GlcNAc synthesis is mediated by GlmS, GlmM and GlmU enzymes. Shaded pathway is conserved in *Mtb*. UDP-GlcNAc can inhibit uridylyltransferase activity by feedback inhibition mechanism. Also GlcNAc from host resources or from cell wall recycling can be transported inside the bacteria and further metabolized and fed into the de novo pathways through GlmS/ GlmU mediated reactions. Question marks show that these pathways are still not characterized in *Mtb*. Dashed lines show possible input of substrates or unknown pathway while complete lines show established and known pathways for UDP-GlcNAc synthesis.

(TIF)

S1 Table. List of bacterial strains, plasmids and phages used in the study.

(DOC)

Acknowledgments

We are grateful to Dr. Rajmani and Tuberculosis Aerosol Challenge Facility (TACF) of ICGB for their support in all animal experiments. We thank the Central Confocal Microscopy, Scanning Electron Microscopy facility, and Biocontainment facility at the National Institute of Immunology, Scanning Electron Microscopy facility at the Advance Instrumentation Research Facility (AIRF) of Jawaharlal Nehru University and Transmission Electron Microscopy Facility at CSIR-Institute of Genomic & Integrative Biology. We thank to Dr. Kalpana Rajanala for her help in confocal imaging. We thank Ms. Rekha Rani and Mr. Mahendra Pratap Singh for their support in SEM/TEM imaging. We thank Dr. Swati Saha for critical reading of the manuscript. We would like to thank Dr. Satyajit Rath, Dr. V. Nagaraja, Dr. T. S. Balganes, Dr. Avinash Bajaj and Dr. Ayub Qadri for scientific discussions and critical inputs.

Author Contributions

Conceived and designed the experiments: VKN VS DS. Performed the experiments: VS PS GS SU AS. Analyzed the data: VKN VS PY DS PS. Wrote the paper: VKN VS PY PS.

References

1. Smith I (2003) Mycobacterium tuberculosis pathogenesis and molecular determinants of virulence. Clin Microbiol Rev 16: 463–496. PMID: [12857778](#)
2. McNeil MR, Brennan PJ (1991) Structure, function and biogenesis of the cell envelope of mycobacteria in relation to bacterial physiology, pathogenesis and drug resistance; some thoughts and possibilities arising from recent structural information. Res Microbiol 142: 451–463. PMID: [1871433](#)
3. Brennan PJ, Nikaido H (1995) The envelope of mycobacteria. Annu Rev Biochem 64: 29–63. PMID: [7574484](#)
4. Lee A, Wu SW, Scherman MS, Torrelles JB, Chatterjee D, et al. (2006) Sequencing of oligoarabinosyl units released from mycobacterial arabinogalactan by endogenous arabinanase: identification of distinctive and novel structural motifs. Biochemistry 45: 15817–15828. PMID: [17176104](#)
5. Zumla A, Nahid P, Cole ST (2013) Advances in the development of new tuberculosis drugs and treatment regimens. Nat Rev Drug Discov 12: 388–404. doi: [10.1038/nrd4001](#) PMID: [23629506](#)
6. Mengin-Lecreulx D, van Heijenoort J (1994) Copurification of glucosamine-1-phosphate acetyltransferase and N-acetylglucosamine-1-phosphate uridylyltransferase activities of Escherichia coli: characterization of the glmU gene product as a bifunctional enzyme catalyzing two subsequent steps in the pathway for UDP-N-acetylglucosamine synthesis. J Bacteriol 176: 5788–5795. PMID: [8083170](#)

7. Gehring AM, Lees WJ, Mindiola DJ, Walsh CT, Brown ED (1996) Acetyltransfer precedes uridylyltransfer in the formation of UDP-N-acetylglucosamine in separable active sites of the bifunctional GlmU protein of *Escherichia coli*. *Biochemistry* 35: 579–585. PMID: [8555230](#)
8. Crick DC, Mahapatra S, Brennan PJ (2001) Biosynthesis of the arabinogalactan-peptidoglycan complex of *Mycobacterium tuberculosis*. *Glycobiology* 11: 107R–118R. PMID: [11555614](#)
9. Alderwick LJ, Birch HL, Mishra AK, Eggeling L, Besra GS (2007) Structure, function and biosynthesis of the *Mycobacterium tuberculosis* cell wall: arabinogalactan and lipoarabinomannan assembly with a view to discovering new drug targets. *Biochem Soc Trans* 35: 1325–1328. PMID: [17956343](#)
10. Barreteau H, Kovac A, Boniface A, Sova M, Gobec S, et al. (2008) Cytoplasmic steps of peptidoglycan biosynthesis. *Fems Microbiology Reviews* 32: 168–207. doi: [10.1111/j.1574-6976.2008.00104.x](#) PMID: [18266853](#)
11. Birch HL, Alderwick LJ, Bhatt A, Rittmann D, Krumbach K, et al. (2008) Biosynthesis of mycobacterial arabinogalactan: identification of a novel alpha(1→3) arabinofuranosyltransferase. *Mol Microbiol* 69: 1191–1206. doi: [10.1111/j.1365-2958.2008.06354.x](#) PMID: [18627460](#)
12. Mills JA, Motichka K, Jucker M, Wu HP, Uhlik BC, et al. (2004) Inactivation of the mycobacterial rhamnosyltransferase, which is needed for the formation of the arabinogalactan-peptidoglycan linker, leads to irreversible loss of viability. *J Biol Chem* 279: 43540–43546. PMID: [15294902](#)
13. Dover LG, Cerdano-Tarraga AM, Pallen MJ, Parkhill J, Besra GS (2004) Comparative cell wall core biosynthesis in the mycolated pathogens, *Mycobacterium tuberculosis* and *Corynebacterium diphtheriae*. *FEMS Microbiol Rev* 28: 225–250. PMID: [15109786](#)
14. Vilcheze C, Av-Gay Y, Attarian R, Liu Z, Hazbon MH, et al. (2008) Mycothiol biosynthesis is essential for ethionamide susceptibility in *Mycobacterium tuberculosis*. *Mol Microbiol* 69: 1316–1329. doi: [10.1111/j.1365-2958.2008.06365.x](#) PMID: [18651841](#)
15. Parikh A, Kumar D, Chawla Y, Kurthkoti K, Khan S, et al. (2013) Development of a new generation of vectors for gene expression, gene replacement, and protein-protein interaction studies in mycobacteria. *Appl Environ Microbiol* 79: 1718–1729. doi: [10.1128/AEM.03695-12](#) PMID: [23315736](#)
16. Verma SK, Jaiswal M, Kumar N, Parikh A, Nandicoori VK, et al. (2009) Structure of N-acetylglucosamine-1-phosphate uridylyltransferase (GlmU) from *Mycobacterium tuberculosis* in a cubic space group. *Acta Crystallogr Sect F Struct Biol Cryst Commun* 65: 435–439. doi: [10.1107/S1744309109010252](#) PMID: [19407371](#)
17. Jagtap PK, Soni V, Vithani N, Jhingan GD, Bais VS, et al. (2012) Substrate-bound crystal structures reveal features unique to *Mycobacterium tuberculosis* N-acetyl-glucosamine 1-phosphate uridylyltransferase and a catalytic mechanism for acetyl transfer. *J Biol Chem* 287: 39524–39537. doi: [10.1074/jbc.M112.390765](#) PMID: [22969087](#)
18. Sassetti CM, Boyd DH, Rubin EJ (2003) Genes required for mycobacterial growth defined by high density mutagenesis. *Mol Microbiol* 48: 77–84. PMID: [12657046](#)
19. Zhang YJ, Ioerger TR, Huttenhower C, Long JE, Sassetti CM, et al. (2012) Global Assessment of Genomic Regions Required for Growth in *Mycobacterium tuberculosis*. *PLoS Pathog* 8: e1002946. doi: [10.1371/journal.ppat.1002946](#) PMID: [23028335](#)
20. Zhang W, Jones VC, Scherman MS, Mahapatra S, Crick D, et al. (2008) Expression, essentiality, and a microtiter plate assay for mycobacterial GlmU, the bifunctional glucosamine-1-phosphate acetyltransferase and N-acetylglucosamine-1-phosphate uridylyltransferase. *Int J Biochem Cell Biol* 40: 2560–2571. doi: [10.1016/j.biocel.2008.05.003](#) PMID: [18573680](#)
21. Jackson M, McNeil MR, Brennan PJ (2013) Progress in targeting cell envelope biogenesis in *Mycobacterium tuberculosis*. *Future Microbiol* 8: 855–875. doi: [10.2217/fmb.13.52](#) PMID: [23841633](#)
22. Moraes GL, Gomes GC, Monteiro de Sousa PR, Alves CN, Govender T, et al. (2015) Structural and functional features of enzymes of *Mycobacterium tuberculosis* peptidoglycan biosynthesis as targets for drug development. *Tuberculosis (Edinb)* 95: 95–111.
23. Urbaniak MD, Collie IT, Fang W, Aristotelous T, Eskilsson S, et al. (2013) A novel allosteric inhibitor of the uridine diphosphate N-acetylglucosamine pyrophosphorylase from *Trypanosoma brucei*. *ACS Chem Biol* 8: 1981–1987. doi: [10.1021/cb400411x](#) PMID: [23834437](#)
24. Moir DT, Di M, Moore RA, Schweizer HP, Woods DE (2008) Cellular reporter screens for inhibitors of *Burkholderia pseudomallei* targets in *Pseudomonas aeruginosa*. *Trans R Soc Trop Med Hyg* 102 Suppl 1: S152–162. doi: [10.1016/S0035-9203\(08\)70033-6](#) PMID: [19121678](#)
25. Pereira MP, Blanchard JE, Murphy C, Roderick SL, Brown ED (2009) High-throughput screening identifies novel inhibitors of the acetyltransferase activity of *Escherichia coli* GlmU. *Antimicrob Agents Chemother* 53: 2306–2311. doi: [10.1128/AAC.01572-08](#) PMID: [19349513](#)

26. Doig P, Boriack-Sjodin PA, Dumas J, Hu J, Itoh K, et al. (2014) Rational design of inhibitors of the bacterial cell wall synthetic enzyme GlmU using virtual screening and lead-hopping. *Bioorg Med Chem* 22: 6256–6269. doi: [10.1016/j.bmc.2014.08.017](https://doi.org/10.1016/j.bmc.2014.08.017) PMID: [25262942](https://pubmed.ncbi.nlm.nih.gov/25262942/)
27. Mochalkin I, Lightle S, Narasimhan L, Bornemeier D, Melnick M, et al. (2008) Structure of a small-molecule inhibitor complexed with GlmU from *Haemophilus influenzae* reveals an allosteric binding site. *Protein Sci* 17: 577–582. doi: [10.1110/ps.073271408](https://doi.org/10.1110/ps.073271408) PMID: [18218712](https://pubmed.ncbi.nlm.nih.gov/18218712/)
28. Buurman ET, Andrews B, Gao N, Hu J, Keating TA, et al. (2011) In vitro validation of acetyltransferase activity of GlmU as an antibacterial target in *Haemophilus influenzae*. *J Biol Chem* 286: 40734–40742. doi: [10.1074/jbc.M111.274068](https://doi.org/10.1074/jbc.M111.274068) PMID: [21984832](https://pubmed.ncbi.nlm.nih.gov/21984832/)
29. Larsen NA, Nash TJ, Morningstar M, Shapiro AB, Joubran C, et al. (2012) An aminoquinazoline inhibitor of the essential bacterial cell wall synthetic enzyme GlmU has a unique non-protein-kinase-like binding mode. *Biochem J* 446: 405–413. doi: [10.1042/BJ20120596](https://doi.org/10.1042/BJ20120596) PMID: [22721802](https://pubmed.ncbi.nlm.nih.gov/22721802/)
30. Min J, Lin D, Zhang Q, Zhang J, Yu Z (2012) Structure-based virtual screening of novel inhibitors of the uridylyltransferase activity of *Xanthomonas oryzae* pv. *oryzae* GlmU. *Eur J Med Chem* 53: 150–158. doi: [10.1016/j.ejmech.2012.03.051](https://doi.org/10.1016/j.ejmech.2012.03.051) PMID: [22521370](https://pubmed.ncbi.nlm.nih.gov/22521370/)
31. Singh VK, Das K, Seshadri K (2012) Kinetic modelling of GlmU reactions—prioritization of reaction for therapeutic application. *PLoS One* 7: e43969. doi: [10.1371/journal.pone.0043969](https://doi.org/10.1371/journal.pone.0043969) PMID: [22952829](https://pubmed.ncbi.nlm.nih.gov/22952829/)
32. Li Y, Zhou Y, Ma Y, Li X (2011) Design and synthesis of novel cell wall inhibitors of *Mycobacterium tuberculosis* GlmM and GlmU. *Carbohydr Res* 346: 1714–1720. doi: [10.1016/j.carres.2011.05.024](https://doi.org/10.1016/j.carres.2011.05.024) PMID: [21704310](https://pubmed.ncbi.nlm.nih.gov/21704310/)
33. Tran AT, Wen D, West NP, Baker EN, Britton WJ, et al. (2013) Inhibition studies on *Mycobacterium tuberculosis* N-acetylglucosamine-1-phosphate uridylyltransferase (GlmU). *Org Biomol Chem* 11: 8113–8126. doi: [10.1039/c3ob41896k](https://doi.org/10.1039/c3ob41896k) PMID: [24158720](https://pubmed.ncbi.nlm.nih.gov/24158720/)
34. Chao MC, Rubin EJ (2010) Letting sleeping dogs lie: does dormancy play a role in tuberculosis? *Annu Rev Microbiol* 64: 293–311. doi: [10.1146/annurev.micro.112408.134043](https://doi.org/10.1146/annurev.micro.112408.134043) PMID: [20825351](https://pubmed.ncbi.nlm.nih.gov/20825351/)
35. Wayne LG, Hayes LG (1996) An in vitro model for sequential study of shutdown of *Mycobacterium tuberculosis* through two stages of nonreplicating persistence. *Infect Immun* 64: 2062–2069. PMID: [8675308](https://pubmed.ncbi.nlm.nih.gov/8675308/)
36. Blokpoel MC, Murphy HN, O'Toole R, Wiles S, Runn ES, et al. (2005) Tetracycline-inducible gene regulation in mycobacteria. *Nucleic Acids Res* 33: e22. PMID: [15687380](https://pubmed.ncbi.nlm.nih.gov/15687380/)
37. Karakousis PC, Williams EP, Bishai WR (2008) Altered expression of isoniazid-regulated genes in drug-treated dormant *Mycobacterium tuberculosis*. *J Antimicrob Chemother* 61: 323–331. PMID: [18156607](https://pubmed.ncbi.nlm.nih.gov/18156607/)
38. Parikh A, Verma SK, Khan S, Prakash B, Nandicoori VK (2009) PknB-mediated phosphorylation of a novel substrate, N-acetylglucosamine-1-phosphate uridylyltransferase, modulates its acetyltransferase activity. *J Mol Biol* 386: 451–464. doi: [10.1016/j.jmb.2008.12.031](https://doi.org/10.1016/j.jmb.2008.12.031) PMID: [19121323](https://pubmed.ncbi.nlm.nih.gov/19121323/)
39. Alavi HA, Moscovic EA (1996) Immunolocalization of cell-wall-deficient forms of *Mycobacterium tuberculosis* complex in sarcoidosis and in sinus histiocytosis of lymph nodes draining carcinoma. *Histol Histopathol* 11: 683–694. PMID: [8839759](https://pubmed.ncbi.nlm.nih.gov/8839759/)
40. BERAN MH V., KAUSTOVA J., DVORSKA L., PAVLIK I. (2006) Cell wall deficient forms of mycobacteria: a review. *Veterinari Medicina* 51: 365–389.
41. Sonnenburg JL, Xu J, Leip DD, Chen CH, Westover BP, et al. (2005) Glycan foraging in vivo by an intestine-adapted bacterial symbiont. *Science* 307: 1955–1959. PMID: [15790854](https://pubmed.ncbi.nlm.nih.gov/15790854/)
42. Renzi F, Manfredi P, Dol M, Fu J, Vincent S, et al. (2015) Glycan-foraging systems reveal the adaptation of *Capnocytophaga canimorsus* to the dog mouth. *MBio* 6: e02507. doi: [10.1128/mBio.02507-14](https://doi.org/10.1128/mBio.02507-14) PMID: [25736888](https://pubmed.ncbi.nlm.nih.gov/25736888/)
43. Renzi F, Manfredi P, Mally M, Moes S, Jenö P, et al. (2011) The N-glycan glycoprotein deglycosylation complex (Gpd) from *Capnocytophaga canimorsus* deglycosylates human IgG. *PLoS Pathog* 7: e1002118. doi: [10.1371/journal.ppat.1002118](https://doi.org/10.1371/journal.ppat.1002118) PMID: [21738475](https://pubmed.ncbi.nlm.nih.gov/21738475/)
44. Gisin J, Schneider A, Nagele B, Borisova M, Mayer C (2013) A cell wall recycling shortcut that bypasses peptidoglycan de novo biosynthesis. *Nat Chem Biol* 9: 491–493. doi: [10.1038/nchembio.1289](https://doi.org/10.1038/nchembio.1289) PMID: [23831760](https://pubmed.ncbi.nlm.nih.gov/23831760/)
45. Engels FK, Mathot RA, Verweij J (2007) Alternative drug formulations of docetaxel: a review. *Anticancer Drugs* 18: 95–103. PMID: [17159596](https://pubmed.ncbi.nlm.nih.gov/17159596/)
46. Coors EA, Seybold H, Merk HF, Mahler V (2005) Polysorbate 80 in medical products and nonimmunologic anaphylactoid reactions. *Ann Allergy Asthma Immunol* 95: 593–599. PMID: [16400901](https://pubmed.ncbi.nlm.nih.gov/16400901/)
47. Lovering AL, Safadi SS, Strynadka NC (2012) Structural perspective of peptidoglycan biosynthesis and assembly. *Annu Rev Biochem* 81: 451–478. doi: [10.1146/annurev-biochem-061809-112742](https://doi.org/10.1146/annurev-biochem-061809-112742) PMID: [22663080](https://pubmed.ncbi.nlm.nih.gov/22663080/)

48. Denholm JT, McBryde ES (2010) The use of anti-tuberculosis therapy for latent TB infection. *Infect Drug Resist* 3: 63–72. PMID: [21694895](#)
49. Hart GW, Slawson C, Ramirez-Correa G, Lagerlof O (2011) Cross talk between O-GlcNAcylation and phosphorylation: roles in signaling, transcription, and chronic disease. *Annu Rev Biochem* 80: 825–858. doi: [10.1146/annurev-biochem-060608-102511](#) PMID: [21391816](#)
50. Tanner ME (2005) The enzymes of sialic acid biosynthesis. *Bioorg Chem* 33: 216–228. PMID: [15888312](#)
51. Itano N, Kimata K (2002) Mammalian hyaluronan synthases. *IUBMB Life* 54: 195–199. PMID: [12512858](#)
52. Swoboda JG, Campbell J, Meredith TC, Walker S (2010) Wall teichoic acid function, biosynthesis, and inhibition. *ChemBiochem* 11: 35–45. doi: [10.1002/cbic.200900557](#) PMID: [19899094](#)
53. Mikusova K, Mikus M, Besra GS, Hancock I, Brennan PJ (1996) Biosynthesis of the linkage region of the mycobacterial cell wall. *J Biol Chem* 271: 7820–7828. PMID: [8631826](#)
54. Skovierova H, Larrouy-Maumus G, Pham H, Belanova M, Barilone N, et al. (2010) Biosynthetic origin of the galactosamine substituent of Arabinogalactan in *Mycobacterium tuberculosis*. *J Biol Chem* 285: 41348–41355. doi: [10.1074/jbc.M110.188110](#) PMID: [21030587](#)
55. Wang X, Quinn PJ (2010) Lipopolysaccharide: Biosynthetic pathway and structure modification. *Prog Lipid Res* 49: 97–107. doi: [10.1016/j.plipres.2009.06.002](#) PMID: [19815028](#)
56. Vimr ER, Kalivoda KA, Deszo EL, Steenbergen SM (2004) Diversity of microbial sialic acid metabolism. *Microbiol Mol Biol Rev* 68: 132–153. PMID: [15007099](#)
57. Dell A, Galadari A, Sastre F, Hitchen P (2010) Similarities and differences in the glycosylation mechanisms in prokaryotes and eukaryotes. *Int J Microbiol* 2010: 148178. doi: [10.1155/2010/148178](#) PMID: [21490701](#)
58. Ujita M, Misra AK, McAuliffe J, Hindsgaul O, Fukuda M (2000) Poly-N-acetylglucosamine extension in N-glycans and core 2- and core 4-branched O-glycans is differentially controlled by i-extension enzyme and different members of the beta 1,4-galactosyltransferase gene family. *J Biol Chem* 275: 15868–15875. PMID: [10747980](#)
59. Alderwick LJ, Molle V, Kremer L, Cozzone AJ, Dafforn TR, et al. (2006) Molecular structure of EmbR, a response element of Ser/Thr kinase signaling in *Mycobacterium tuberculosis*. *Proc Natl Acad Sci U S A* 103: 2558–2563. PMID: [16477027](#)
60. Gill WP, Harik NS, Whiddon MR, Liao RP, Mittler JE, et al. (2009) A replication clock for *Mycobacterium tuberculosis*. *Nat Med* 15: 211–214. doi: [10.1038/nm.1915](#) PMID: [19182798](#)
61. Naseem S, Parrino SM, Buenten DM, Konopka JB (2012) Novel roles for GlcNAc in cell signaling. *Commun Integr Biol* 5: 156–159. doi: [10.4161/cib.19034](#) PMID: [22808320](#)
62. Handford M, Rodriguez-Furlan C, Orellana A (2006) Nucleotide-sugar transporters: structure, function and roles in vivo. *Braz J Med Biol Res* 39: 1149–1158. PMID: [16981043](#)
63. Konopka JB (2012) N-acetylglucosamine (GlcNAc) functions in cell signaling. *Scientifica (Cairo)* 2012.
64. Klotzsche M, Ehart S, Schnappinger D (2009) Improved tetracycline repressors for gene silencing in mycobacteria. *Nucleic Acids Res* 37: 1778–1788. doi: [10.1093/nar/gkp015](#) PMID: [19174563](#)
65. Jain P, Hsu T, Arai M, Biermann K, Thaler DS, et al. (2014) Specialized transduction designed for precise high-throughput unmarked deletions in *Mycobacterium tuberculosis*. *MBio* 5: e01245–01214. doi: [10.1128/mBio.01245-14](#) PMID: [24895308](#)
66. Bardarov S, Bardarov S Jr, Jr., Pavelka MS Jr, Jr., Sambandamurthy V, Larsen M, et al. (2002) Specialized transduction: an efficient method for generating marked and unmarked targeted gene disruptions in *Mycobacterium tuberculosis*, *M. bovis* BCG and *M. smegmatis*. *Microbiology* 148: 3007–3017. PMID: [12368434](#)
67. Chawla Y, Upadhyay S, Khan S, Nagarajan SN, Forti F, et al. (2014) Protein kinase B (PknB) of *Mycobacterium tuberculosis* is essential for growth of the pathogen in vitro as well as for survival within the host. *J Biol Chem* 289: 13858–13875. doi: [10.1074/jbc.M114.563536](#) PMID: [24706757](#)
68. Gupta A, Sharma Y, Dash KN, Verma S, Natarajan VT, et al. (2014) Ultrastructural Investigations in an Autosomal Recessively Inherited Case of Dyschromatosis Universalis Hereditaria. *Acta Derm Venereol*.
69. Pandey AK, Raman S, Proff R, Joshi S, Kang CM, et al. (2009) Nitrile-inducible gene expression in mycobacteria. *Tuberculosis (Edinb)* 89: 12–16.
70. Ehart S, Guo XV, Hickey CM, Ryou M, Monteleone M, et al. (2005) Controlling gene expression in mycobacteria with anhydrotetracycline and Tet repressor. *Nucleic Acids Res* 33: e21. PMID: [15687379](#)

71. Puri RV, Reddy PV, Tyagi AK (2013) Secreted acid phosphatase (SapM) of *Mycobacterium tuberculosis* is indispensable for arresting phagosomal maturation and growth of the pathogen in guinea pig tissues. *PLoS One* 8: e70514. doi: [10.1371/journal.pone.0070514](https://doi.org/10.1371/journal.pone.0070514) PMID: [23923000](https://pubmed.ncbi.nlm.nih.gov/23923000/)
72. Hu Y, Coates AR (2009) Acute and persistent *Mycobacterium tuberculosis* infections depend on the thiol peroxidase TpX. *PLoS One* 4: e5150. doi: [10.1371/journal.pone.0005150](https://doi.org/10.1371/journal.pone.0005150) PMID: [19340292](https://pubmed.ncbi.nlm.nih.gov/19340292/)
73. Reddy PV, Puri RV, Chauhan P, Kar R, Rohilla A, et al. (2013) Disruption of mycobactin biosynthesis leads to attenuation of *Mycobacterium tuberculosis* for growth and virulence. *J Infect Dis* 208: 1255–1265. doi: [10.1093/infdis/jit250](https://doi.org/10.1093/infdis/jit250) PMID: [23788726](https://pubmed.ncbi.nlm.nih.gov/23788726/)
74. Kirchmair J, Distinto S, Markt P, Schuster D, Spitzer GM, et al. (2009) How to optimize shape-based virtual screening: choosing the right query and including chemical information. *J Chem Inf Model* 49: 678–692. doi: [10.1021/ci8004226](https://doi.org/10.1021/ci8004226) PMID: [19434901](https://pubmed.ncbi.nlm.nih.gov/19434901/)
75. Hawkins PC, Skillman AG, Nicholls A (2007) Comparison of shape-matching and docking as virtual screening tools. *J Med Chem* 50: 74–82. PMID: [17201411](https://pubmed.ncbi.nlm.nih.gov/17201411/)
76. György Kóczána GCK, Antal Csámpaic, Balogh Erika, Szilvia Bőszea Pál Sohár, Hudecza Ferenc (2001) Synthesis and characterization of 4-ethoxymethylene-2-[1]-naphthyl-5(4H)-oxazolone and its fluorescent amino acid derivatives *Tetrahedron* 57: 4589–4598.
77. William L. Jorgensen DSM, and Julian Tirado-Rives (1996) Development and Testing of the OPLS All-Atom Force Field on Conformational Energetics and Properties of Organic Liquids. *Journal of the American Chemical Society* 118: 11225–11236.
78. William L. Jorgensen JC, Jeffrey D. Madura, Impey Roger W. and Klein Michael L. (1983) Comparison of simple potential functions for simulating liquid water. *The Journal of Chemical Physics* 79: 926–935.
79. Vincent Kräutler WFvGaHH(2001) A fast SHAKE algorithm to solve distance constraint equations for small molecules in molecular dynamics simulations. *Journal of Computational Chemistry* 22: 501–508.
80. Zhou Y, Xin Y, Sha S, Ma Y (2011) Kinetic properties of *Mycobacterium tuberculosis* bifunctional GImU. *Arch Microbiol* 193: 751–757. doi: [10.1007/s00203-011-0715-8](https://doi.org/10.1007/s00203-011-0715-8) PMID: [21594607](https://pubmed.ncbi.nlm.nih.gov/21594607/)